THE JOURNAL OF COMPARATIVE NEUROLOGY 288:59–80 (1989)

Monoamine-Accumulating Ganglion Cell Type of the Cat's Retina

DENNIS M. DACEY
Department of Biological Structure, The University of Washington, Seattle, Washington 98195

ABSTRACT

A monoamine-accumulating ganglion cell type has been identified in an in vitro preparation of the cat's retina by a catecholamine-like fluorescence that appears following intravitreal injections of dopamine and the indoleaminergic transmitter analog, 5,7-dihydroxytryptamine (5,7-DHT). A subpopulation of large, weakly fluorescing neurons were identified as composing a single, morphologically distinct ganglion cell type by intracellular injections of horseradish peroxidase (HRP). In a sample of 374 HRP-filled cells soma diameter ranged from 13–21 μm (mean ± SD = 16.6 ± 1.3). Dendritic field size increased with increasing retinal eccentricity from 150–200 μm diameter at 0.5 mm from the area centralis to 600–800 μm diameter in the far retinal periphery. Dendrites are thin (~1 μm diameter), show a characteristic branching pattern, and are narrowly stratified at the outer border of the inner plexiform layer. The monoamine-accumulating ganglion cell and the outer (OFF-center) alpha cell occupy distinct strata within sublamina a of the inner plexiform layer separated by a gap of about 5 μm.

The total number of monoamine-accumulating (MA) ganglion cells was estimated at 5,400, about 3.5% of the total ganglion cell population. Spatial density of the MA ganglion cells, calculated from cell counts made in vitro, ranges from 60 cells/mm^2 near the area centralis to 5 cells/mm^2 in the far retinal periphery. A coverage factor (density × dendritic field area) of 2.2 was maintained from central to peripheral retina. The nature of the dendritic overlap was observed directly by making HRP injections into several neighboring ganglion cells. Five to seven neighboring dendritic trees extensively overlapped a given cell's dendritic field. However the dendritic processes did not intersect randomly but tended to interdigitate such that a uniform interdendritic spacing and density of dendritic processes was constructed locally within the dendritic plexus. Rotation of individual dendritic trees from their normal orientation produced a dramatic 4–5-fold increase in the number of dendritic intersections, suggesting that an active, local mechanism operates in the precise placement of individual dendrites within the plexus.

The monoamine-accumulating ganglion cell appears morphologically equivalent to the delta ganglion cell (Boycott and Wässle; *J. Physiol. (Lond.) 240*:397–419, '74; Kolb et al.; *Vision Res. 21*:1081–1114, '81) and to the recently recognized indoleamine-accumulating ganglion cell (Wässle et al: *J. Neurosci. 7*:1574–1585, '87). Comparisons with previous studies indicate that they may be physiologically equivalent to the OFF-center, sluggish sustained cells (also known as tonic W cells and Q cells) and probably project to the superior colliculus and/or the C-lamina of the dorsal lateral geniculate nucleus.

Key words: dopamine, serotonin, in vitro, horseradish peroxidase, catecholamine fluorescence, coverage factor

Accepted May 9, 1989.

In the vertebrate retina, the number of functionally distinct ganglion cell types is thought to be roughly 20, yet the *identification* and detailed study of individual types remain a difficult problem. An important step toward the identification of ganglion cell types has been to label selectively an entire subpopulation of neurons of a given type, and to demonstrate that each subpopulation forms an independent network of dendritic trees that economically tiles the retinal surface. In the cat's retina only four cell types, the ON- and OFF-center X-beta and Y-alpha cells have been recognized by this criterion (Wässle et al., '81a,b). The two alpha cell subpopulations were identified by a silver stain selective for their dendritic trees and the beta cells were identified by retrograde labeling from tracer injections in the A-laminae of the dorsal lateral geniculate nucleus. Differences in morphology and receptive field properties (e.g., Cleland and Levick, '74a,b; Leventhal et al., '80; Kolb et al., '81; Dacey, '84; Rodieck and Watanabe, '86) indicate the existence of many other ganglion cell types in the cat's retina, but definitive evidence for multiple, unique ganglion cell subpopulations beyond the alpha and beta cell types is lacking.

Recently the use of cell-type-specific markers has permitted the identification and morphological analysis of retinal cell populations by intracellular injections of the fluorescent dye Lucifer yellow under direct microscopic control in aldehyde-fixed tissue (Tauchi and Masland, '84). Formaldehyde-induced histofluorescence has been used to mark catecholaminergic and indoleaminergic amacrine cell subpopulations in the cat and rabbit retina (Tauchi and Masland, '86; Sandell and Masland, '86; Wässle et al., '87; Voigt and Wässle, '87). In the cat retina indoleamine histofluorescence (induced by uptake of 5,7-DHT) also was observed in ganglion cells (Wässle et al., '87). Intracellular injections of Lucifer yellow suggested the possibility that these cells composed a single morphologically distinct ganglion cell subpopulation not previously studied in detail. In the present study combined uptake of dopamine and 5,7-DHT was used to produce an intense monoamine-like fluorescence in an in vitro preparation of the cat's retina (Dacey, '88). Under the appropriate conditions a ganglion cell population can be observed that appears to correspond to the indoleamine-accumulating ganglion cells observed by Wässle et al. ('87) in fixed tissue (Dacey, '87). The in vitro fluorescence permitted intracellular injections of HRP into these cells and subsequent analysis of their morphology and retinal distribution. The results show that they form a single, morphologically distinct ganglion cell subpopulation with a characteristic retinal topography, dendritic field size and stratification, and mosaic organization.

MATERIALS AND METHODS

Twenty-nine adult cats were used for this study. Each animal was initially sedated with xylazine (Rompun, 1 mg/kg, I.M.) and then deeply anaesthetized with halothane (1.5%) and equal parts nitrous oxide and oxygen (2 liters/minute). This level of gaseous anaesthesia was maintained throughout the course of the experiment via a tracheal catheter. The heart rate was stabilized with atropine sulfate (1 mg/kg, I.M.) and the electrocardiogram was continuously monitored. Body temperature was monitored via a rectal thermistor and maintained in the physiological range (36–38°C) by a heating blanket. To prevent the degradation of dopamine, 5 animals also received the monoamine oxidase (MAO) inhibitor Pargyline (5–50 mg/kg, I.P.) and the catechol-o-methyltransferase (COMT) inhibitor Pyrogallol (5–50 mg/kg, I.P.). The resulting in vitro fluorescence did not appear to be increased over the cases in which inhibitors of dopamine breakdown were not used. At the end of each experiment, the animal was killed with an overdose of sodium pentobarbital (Nembutal, 50 mg, I.V.) while still under deep gaseous anaesthesia.

For drug injections, the animal's head was fixed in a stereotaxic frame to facilitate surgery. The sclera of the eye was exposed by making an incision in the skin along the lateral margin of the eye, removing the surrounding conjunctiva and connective tissue, and cutting the intraocular muscles. A 30-gauge needle attached to a Hamilton syringe was used to make the injections. Initially 100–200 μl of a solution containing dopamine (10 μg/μl) and 5,7-dihydroxytryptamine (1 μg/μl) in physiological saline with ascorbic acid (1 mg/ml) added as an antioxidant was injected into the vitreous over a period of 5 minutes. It was found that the resulting in vitro fluorescence (see Results) was restricted to a circular region of the retina a few mm in diameter centered around the injection site. In subsequent experiments the same total volume was injected into the vitreous by making up to ten and 20 μl injections at evenly spaced intervals around the circumference of the eye. This resulted in a more even distribution of fluorescence over the entire retina.

Both the right and left eyes were injected in this way. Three to 5 hours later the right eye was dissected from the orbit. The eye was hemisected at the corneoscleral junction and the vitreous was removed. The eyecup was then placed in Ames medium (Ames and Nesbett, '81) and continuously oxygenated (95% O_2/5% CO_2). The retina was dissected from the eyecup, care being taken to remove any excess vitreous from the retinal surface. A series of radial cuts were made in the retina, and it was mounted flat, vitreal side uppermost in a superfusion chamber on the stage of a light microscope equipped for episcopic illumination. The superfusion chamber was fashioned from a plastic ring glued to a microscope slide. Warm 30% gelatin was poured into the chamber so as to thinly cover its bottom and was allowed to congeal slightly at room temperature. The retina was then laid flat on the gelatin to which it lightly adhered. The entire retinal surface can be easily viewed in this way with either transmitted or episcopic illumination while being continuously superfused with oxygenated Ames medium. Retinas were maintained for several hours at room temperature with no apparent deterioration in cellular morphology at the light microscopic level. When experiments using the first eye were complete (usually within 3–4 hours) the second eye was removed and the retina was prepared in the same way.

Intracellular microelectrodes were formed from thin-walled microcapillary glass pulled to an initial resistance of about 175–250 MΩ on a Brown-Flaming micropipette puller. The electrodes were filled with a 4% solution of rhodamine-conjugated HRP (Sigma) and Lucifer yellow (Aldrich) in Tris buffer (pH 7.6) and beveled to a final resistance of 80–150 MΩ.

The epifluorescence microscope used to observe the in vitro fluorescence was equipped with a micromanipulator mounted on the base of the microscope stage such that a microelectrode could be positioned independently of focus (stage height). An oil-driven microdrive mounted to the manipulator was used to advance the microelectrode tip manually. Both the electrode tip and the retina were viewed together at high resolution with a 40× water-immersion, long working distance objective that was modified to permit the proper angle of electrode approach to the tissue (Brown and Flaming, '86).

Both Lucifer yellow fluorescence in the electrode and the monoamine-like fluorescence in the tissue were observed with the same filter combination (excitation filter, 410–490 nm; barrier filter 515 nm long pass). This permitted the electrode tip to be positioned near the fluorescing cell under direct microscopic control. Cell penetration was achieved by tapping the base of the microscope and was subsequently confirmed by observing the target cell after brief iontophoresis of Lucifer yellow with negative current (0.1–1.0 namp for 5–10 seconds). If the penetration was successful the cell was then injected with rhodamine-conjugated HRP by passing positive current (3–8 namps; 1–3 minutes). The accumulation of rhodamine-HRP in the cell and the quality of the cell's morphology were directly assessed by observing the red fluorescing rhodamine (excitation filter, 545 nm; barrier filter, 590 nm), which appeared to slowly increase in brightness and fill the cell's processes during the course of the injection. Multiple cells were injected over a 2–4-hour period; the retina was then removed from the superfusion chamber and fixed in phosphate-buffered 1% glutaraldehyde (0.1 M; pH 7.4) for 2 hours. HRP reaction product was demonstrated in the intact retinal wholemounts by using diaminobenzidine as the chromagen according to a standard protocol (Dacey, '85a). For subsequent light microscopic analysis the retinas were mounted on slides vitreal side up, dehydrated, cleared, and coverslipped.

Soma and dendritic field sizes were determined for a sample of 374 cells, which appeared to be completely filled by the HRP injection. The dendrites of these cells showed a dark and uniform reaction product out to their distal dendritic tips. Cells judged to be incompletely filled were more lightly stained and showed nonuniform filling marked by gradual fading of the HRP reaction product from the proximal to distal dendritic tree. Soma area was determined by making camera lucida tracings of cell bodies at 1,500 times magnification which were then entered into a computer via a graphics tablet. Soma diameter was expressed as the diameter of a circle having the same area. To calculate the dendritic field area, a convex polygon was traced around the dendritic field perimeter of each cell and entered into a computer via a graphics tablet. The best-fitting ellipse having the same area was also calculated. Dendritic field diameter was expressed as the diameter of a circle having the same area as that of the ellipse.

For one cell the depth of stratification for the entire dendritic tree in a wholemounted retina was determined by making a camera lucida tracing with a computer system that preserved Z-axis information (Eutectics Neuron Tracing System). The dendritic tree was then rotated by 90° to give its depth of stratification. Shrinkage in the retina was estimated at 70% by comparing a measurement of the IPL thickness taken from the in vitro retina with that taken from the same retina after fixation, mounting, and dehydration. The Z-axis was expanded by this percentage to give the depth of stratification. The stratification for 51 other HRP-filled cells was determined alternatively by reading the scale on the focus knob of the microscope (Olympus BH-2, calibrated to 1 μm intervals). First, the thickness of the IPL was estimated by taking a reading of the focal plane of the HRP-filled soma and the inner border of the inner nuclear layer. Measurement of IPL thickness made in this way was consistently 11–12 μm in dehydrated retinas. A reading of the plane of focus of the region of the dendritic tree directly overlying the soma was then taken and depth of stratification was expressed as a percentage of the total thickness of the IPL. This method was also used in one other case to compare the depths of stratification of two ganglion cells with overlapping dendritic fields: one was an MA ganglion cell and the other was an outer-alpha cell that had also been intracellularly injected with HRP.

Counts were made of the fluorescing ganglion cells in a single retina while it was maintained in vitro. The counts were made by using a 40× water immersion objective. The field size was 250 μm^2 and was projected onto the microscope field with the aid of a drawing tube. Eight contiguous fields were sampled to provide a count over an area of 0.5 mm^2 at each location sampled. A total of 104 locations were sampled at approximately 2 mm intervals.

RESULTS

Identification of the monoamine-accumulating ganglion cell type by in vitro fluorescence

Several hours following intravitreal injections of DA and 5,7-DHT, an intense yellow-green fluorescence could be observed in cell bodies in the inner nuclear layer and ganglion cell layer and in dendritic trees and fine varicose processes in the inner plexiform layer (Fig. 1). The intensity and total extent of the in vitro fluorescence developed slowly over a characteristic time course. The development of the fluorescence was followed by observing retinas beginning 1 hour after intravitreal injection. At this time the fluorescence was limited to varicosities and fine processes in the IPL and was relatively weak and easily quenched under blue excitation; no fluorescing cell bodies were usually observed. Over the next 2 hours the intensity and extent of the fluorescence increased and became more stable. Between 2 and 3 hours postinjection weak fluorescence first appeared in large cell bodies in the inner nuclear layer (Fig. 1A). Over the next few hours the fluorescence continued to increase dramatically such that these cell bodies and their dendritic trees became intensely fluorescent and stood out against a background of fine varicose processes (Fig. 1B,C). During this time cell bodies in the ganglion cell layer and their processes also began to fluoresce. Finally, between 5 and 7 hours, a distinct population of large (~20 μm diam) fluorescent cell bodies could be observed in the ganglion cell layer (Fig. 1D, arrow). In addition to their larger size these cells could easily be distinguished from the earlier fluorescing cells by a relatively weak fluorescence that was restricted to the cell body (Fig. 1D). Intracellular injections of HRP into the fluorescing cells in the ganglion cell layer showed that the large, weakly fluorescent cells composed a single, morphologically distinct ganglion cell type and that the smaller, more intensely fluorescent cell types were amacrine cells. In this report the morphology and topographic distribution of these monoamine-accumulating (MA) ganglion cells is presented.

Dendritic morphology

The characteristic dendritic morphology of the MA ganglion cell shown by intracellular injection of HRP is illustrated in Figures 2 and 3. Dendrites are moderately branched and follow a wavy or meandering course and only occasionally overlap. They do not obviously taper but show a fairly constant diameter (~1 μm) through 3–5 orders of branching (Figs. 2A,C,D, 3A). Primary dendrites arise from the soma and extend vertically towards the outer margin of the inner plexiform layer before branching (Figs. 2B, 3B). The second- and higher-order branches are easily observed in a single focal plane (Fig. 2C,D) and appear to be narrowly

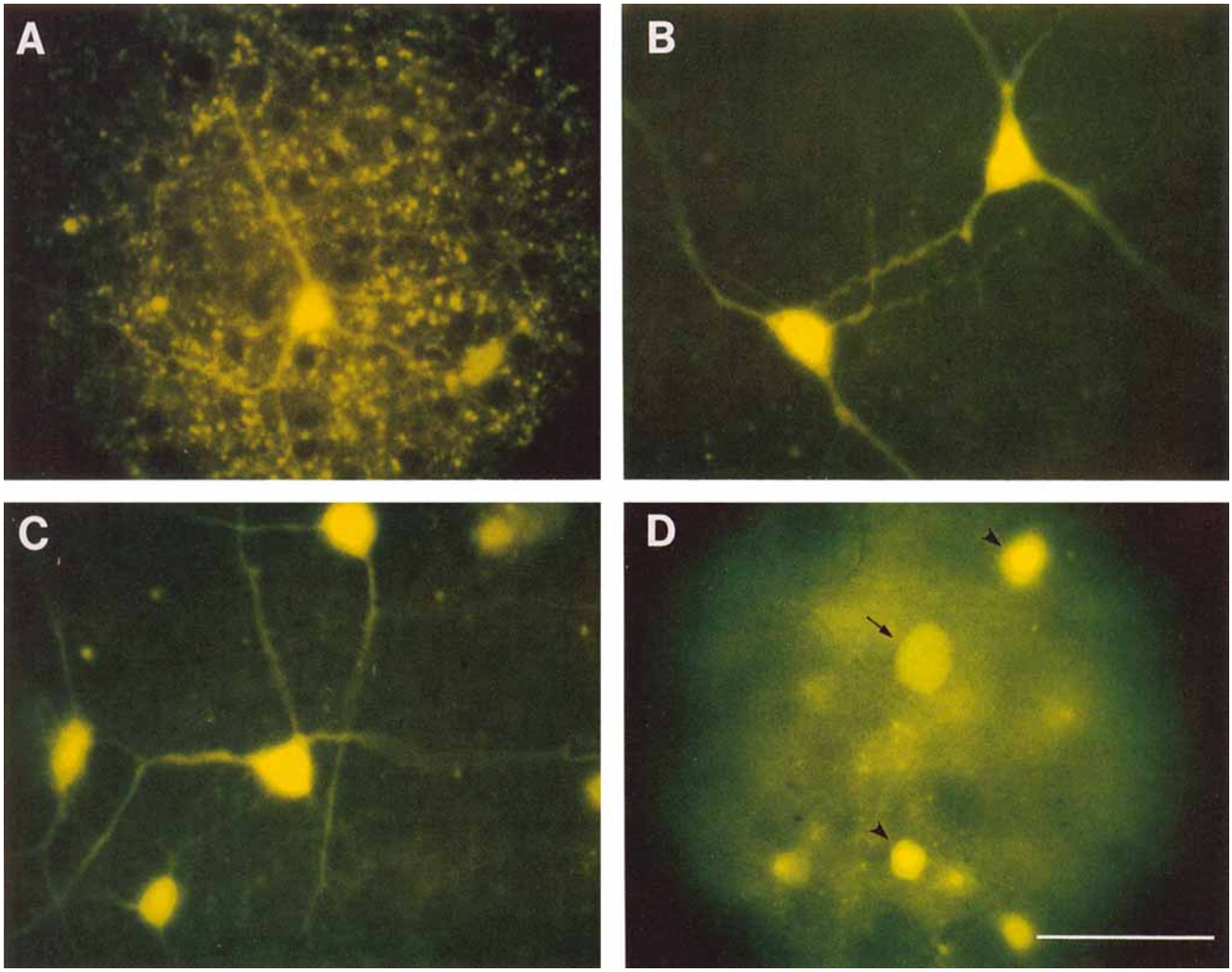

Fig. 1. In vitro fluorescence following intravitreal injections of dopamine and 5,7-DHT. **A:** Fluorescing plexus of varicosities and fine processes at the outer border of the inner plexiform layer. A large fluorescing cell and its major dendrites are slightly out of the plane of focus. **B** and **C:** Fluorescence in amacrine cell somata in the inner nuclear layer and their dendrites in the inner plexiform layer. In these micrographs fluorescence in the dense plexus of varicosities and very fine processes has been quenched to some degree by previous exposure to blue light, revealing more clearly the fluorescing amacrine cell dendritic trees. **D:** Fluorescence in the ganglion cell layer. Small amacrine cells (arrowheads) show intense fluorescence in their soma. A ganglion cell shows weaker fluorescence that is restricted to the soma (arrow). Scale bar = 50 μm.

stratified at the outer border of the inner plexiform layer, adjacent to the amacrine cell sublayer of the inner nuclear layer (Fig. 3B). The dendrites are not particularly smooth but show irregular contours marked by slight constrictions, swellings, and other irregular protrusions. The complexity of the dendritic tree is further increased by a moderate covering of spine-like extensions and small branchlets (Figs. 2C,D, 3A).

Dendritic field and soma size

Approximately 500 MA ganglion cells were injected with HRP to provide a sample for a more detailed analysis of the morphology of the MA ganglion cell subpopulation. Cells that showed complete HRP filling like that illustrated in Figures 2 and 3 were included in the sample (n = 374). Cells were excluded if they showed any signs of damage or degeneration (such as beaded or broken dendrites) or if the HRP labeling appeared weak or faded in the distal dendritic tree. By contrast, well-filled cells were darkly stained with the HRP reaction product and the distal dendrites could easily be traced to what appeared to be their natural endpoints (e.g., Figs. 2A, 3A).

The dendritic fields of the MA ganglion cells showed a clear increase in size with increasing distance from the area centralis. Examples of the dendritic trees of cells from central, midperipheral, and far-peripheral retina are illustrated in Figures 4–6. The basic branching pattern and structure of the dendritic tree that is characteristic of the MA cell type was identifiable at each of these eccentricities. Inspection of the branching pattern of the cells shown in Figures 4–6 suggests that the 5–6-fold increase in dendritic field size was accomplished principally by an increase in the length of

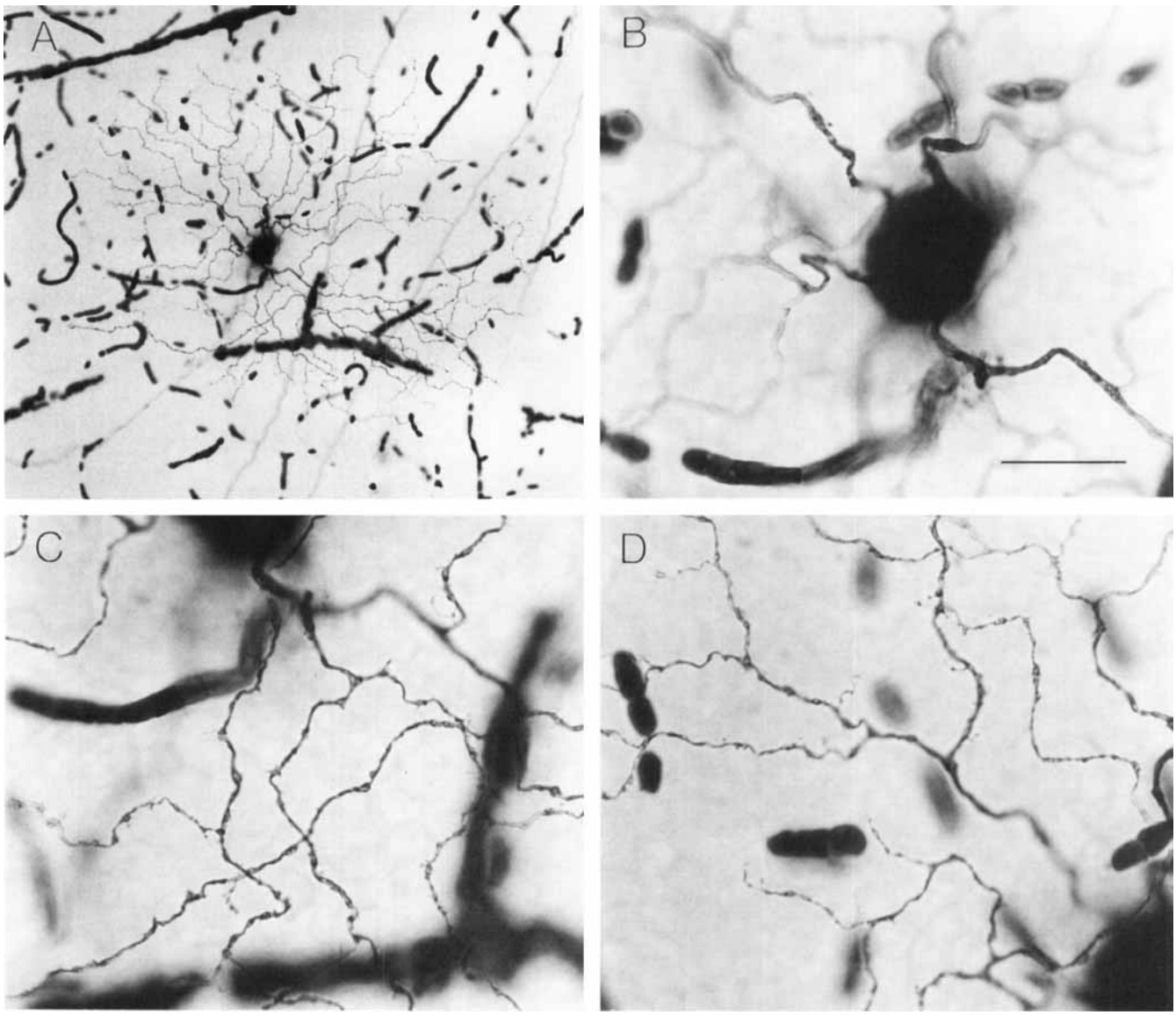

Fig. 2. Intracellular HRP injections of monoamine-accumulating (MA) ganglion cells. **A:** The entire dendritic tree of a single MA ganglion cell is shown at low magnification (×190) in a wholemount preparation following HRP histochemistry with diaminobenzidine (DAB) as the chromagen. **B:** Primary dendrites descend obliquely and turn to occupy a narrow stratum at the outer border of the inner plexiform layer. **C** and **D:** Dendrites are thin and meandering; occasional swellings, spine-like processes, and short branchlets are evident. A complete camera lucida tracing of the cell shown in this figure is illustrated in Figure 3. Scale bar = 20 μm and applies to panels B–D.

dendrites between branchpoints without a corresponding change in the number of branchpoints within the dendritic tree. Thus peripheral cells (Fig. 6A,B) had the appearance of being more sparsely branched than central cells (e.g., Fig. 4) because a similar number of branch points were dispersed over a much larger field area.

To determine whether the number of dendritic branches may be a characteristic feature of the MA cell type that is independent of size, branchpoints were counted in a sample of 13 completely traced cells from a range of retinal eccentricities (10 of those cells are illustrated in the Figs. 3–6 and 15). The mean number of branchpoints for these cells was 63 (SD = 13; range 42–79). The extremes in the range of branchpoint number were observed in cells with very similar dendritic field sizes. For example, the cell at 1.5 mm eccentricity (Fig. 4A) had 48 branchpoints and a cell of about the same size at 2.0 mm eccentricity (Fig. 3) had 77 branch points. However, a scatterplot of dendritic field size as a function of the number of dendritic branchpoints (Fig. 7) suggests a small but significant increase in branchpoint number with increasing dendritic field size. There thus appears to be a weak tendency for the larger cells to show a greater number of dendritic branchpoints, but it is a relatively small increase compared to the large increase in dendritic field size.

The relationship of dendritic field size to retinal eccentricity for the entire sample is shown in the scatterplot in Figure 8A. The dendritic field diameter ranged from ~150

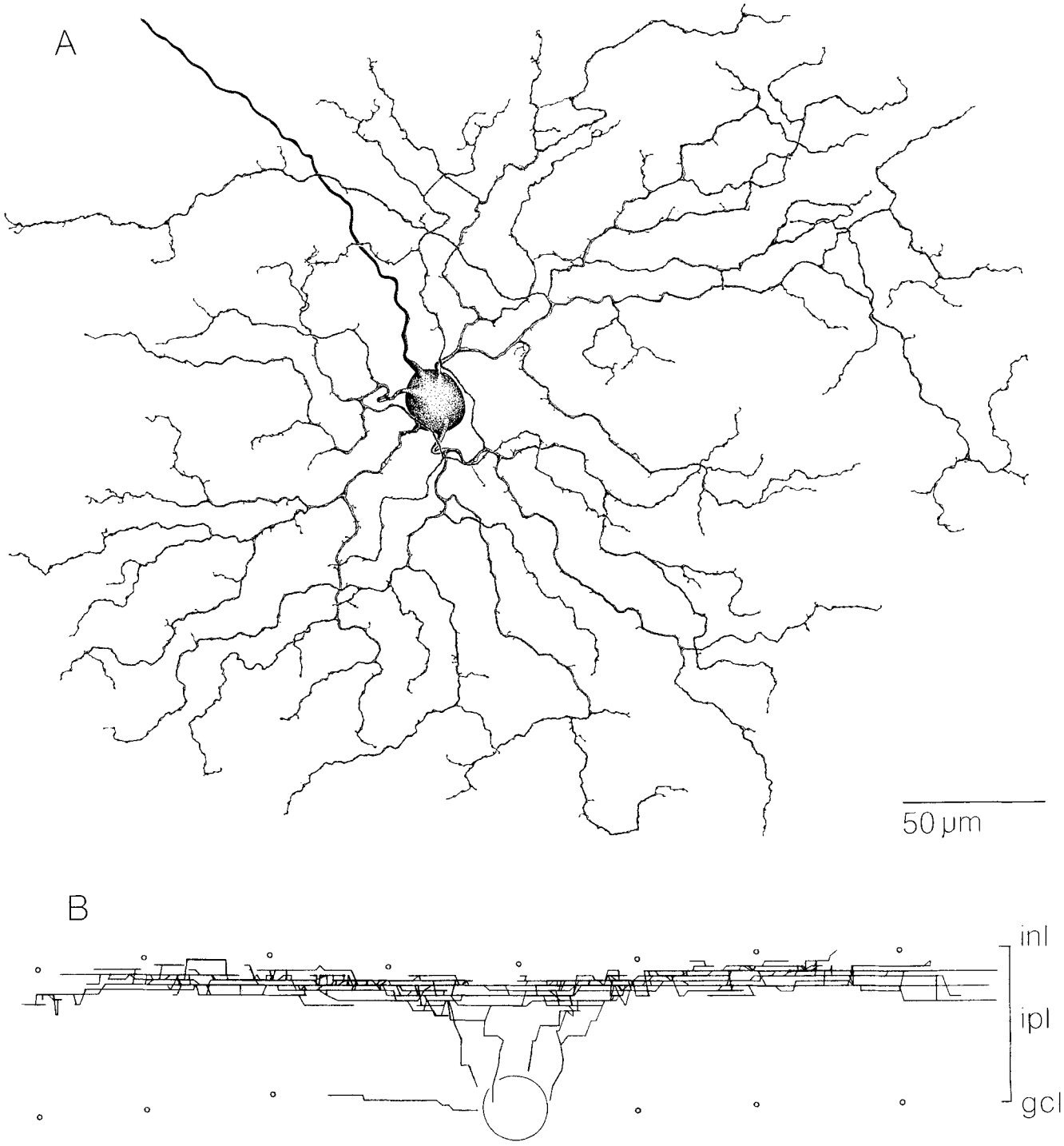

Fig. 3. Dendritic morphology of the MA ganglion cell type. **A:** Camera lucida tracing of the cell shown in Figure 2. Dendrites are thin (~1 µm), moderately branched, and follow a wavy or meandering course and only occasionally overlap. Dendrites show a moderate covering of spine-like structures and small branchlets (see also Fig. 2C,D). **B:** 90° rotation of the dendritic tree of the cell shown in A illustrates a narrow depth of stratification near the outer border of the inner plexiform layer (ipl) for most second- and higher-order branches. The Z-axis has been expanded by 70% by the computer prior to rotation to compensate for the estimated vertical shrinkage of the retina caused by dehydration. inl, gcl, inner nuclear and ganglion cell layers.

μm (at 0.5 mm from the area centralis) to ~800 μm (at 14 mm from the area centralis). No cells were successfully recovered from within 0.5 mm of the area centralis (although the fluorescing somata of the MA cells could often be observed in this region). It is therefore possible that within the region of highest cell density dendritic fields of the MA cells have a diameter of less than 150 μm. Field size was strongly correlated with distance from the area centralis ($R = 0.78$; $P < 0.001$). The MA ganglion cell thus showed a progressive increase in dendritic field size from central to peripheral retina similar to that reported for alpha cells which range from about 200 to 1,000 μm in diameter (Boycott and Wässle, '74; Wässle et al., '81b). However, at all eccentricities the MA cells are smaller by about 40% in dendritic field area than the alpha cells.

Soma diameters of the MA ganglion cells ranged from 13–21 μm with a mean of 16.6 μm ($n = 374$; SD = 1.3 μm) (Fig. 8B). Some of the smallest somata were observed within 1 mm of the area centralis. However, Figure 6B also shows that roughly the full soma size range was present at any given eccentricity. Observations made during electrode penetration and intracellular injection suggested that the scatter of soma sizes should be interpreted with caution. It was evident that in some instances soma size and shape appeared to be altered by electrode penetration and current injection. The most common observation was that the soma would appear to swell during the injection period. Less commonly, an electrode penetration might distort the apparent shape of soma or lead to a decrease in apparent size. It is not known whether these observations made during the in vitro period led to permanent changes in soma size and shape after fixation and HRP histochemistry, but it is certainly possible that trauma to the soma due to electrode penetration could contribute to the scatter in the soma size range.

Dendritic stratification

The dendritic tree of the MA ganglion cell was narrowly stratified close to the outer border of the inner plexiform layer. Measurements taken in vitro from Lucifer yellow–filled cells showed that the dendritic tree consistently arborized 25–30 μm from the cell body, adjacent to the amacrine cell sublayer of the inner plexiform layer. These observations were confirmed by making a camera lucida tracing of Figure 9B, (shown in Figs. 2 and 3) with a computer system designed to preserve depth information. A 90° rotation of this cell also showed that the main arborization of the dendritic tree was restricted to the outer border of the inner plexiform layer (Fig. 3B). This finding was extended to a larger sample by measuring the stratification of the dendritic tree relative to the total thickness of the inner plexiform layer for each of 51 HRP-filled cells. Level of dendritic stratification was estimated in the retinal wholemounts by measuring the relative depth of the focal plane of the dendritic tree and the borders of the ganglion cell layer and inner nuclear layer (Fig. 10A). The results, expressed as percent distance from the ganglion cell layer, gave a mean depth of 85% (range = 82–92%, SD = 3.3%).

The stratification of the MA ganglion cell was further specified by comparing the relative depths of the dendrites of an outer-alpha cell and an MA cell. Previous studies of the stratification of the outer-alpha cells show that they are narrowly stratified close to the center of the inner plexiform layer (Famiglietti and Kolb, '76; Wässle et al., '81b; Freed and Sterling, '88). This suggests that the outer-alpha cell and the MA cell occupy different levels of stratification within the outer portion of the inner plexiform layer. This prediction was tested by injecting pairs of MA and outer-alpha cells. An MA cell was first injected with HRP; the soma of the nearest alpha cell (identified with transmitted light by its large size) was then injected with Lucifer yellow. If the alpha cell clearly extended dendrites into the outer portion of the inner plexiform layer, it was subsequently injected with HRP through the same electrode. In a few cases, pairs of MA and outer-alpha cells with highly overlapping dendritic fields were successfully recovered (e.g., Fig. 9A) and their relative depths of stratification could be directly observed (Fig. 9B,C). For the alpha/MA cell pair shown in Figure 9 the relative stratification was determined as for the previous MA cell sample (Fig. 10A) except that depth readings were taken at all locations where an MA cell dendrite and an alpha cell dendrite overlapped. The results, shown in the histogram in Figure 10B, confirm again the level of stratification of the MA cell. In addition the outer-alpha cell was narrowly stratified about 15% further vitread in the inner plexiform layer, resulting in a gap between the strata for the two cell types of about 5 μm in unfixed tissue.

Topographic distribution

The number and topographic distribution of the MA ganglion cells was determined by counting fluorescing cells while the retina was maintained in vitro. This was a time-consuming task and because fixation of the retina quenched the fluorescence it was not possible to make a large number of counts nor to confirm counts by later reexamination. Cells were sampled at 2 mm intervals along vertical transects from dorsal to ventral retina; adjacent transects were also separated by 2 mm intervals (Fig. 11A). In a few instances counts were made at 1.5 mm intervals near the area centralis. A total of 104 locations were successfully sampled. Several locations were not sampled because of damage to the retina over some part of the field incurred from the intravitreal drug injections or from the retinal dissection. Cells were counted within eight adjacent fields, 250 μm on a side, to provide a total sample area 0.5 mm^2 at each sample site. The field was observed through a camera lucida attachment and adjacent fields were aligned by using blood vessels or the distinctive pattern of fluorescing processes in the inner plexiform layer.

Cell counts were plotted on a tracing of the retina and isodensity contour lines were fit by eye to provide a picture of the overall density distribution for the MA ganglion cells (Fig. 11B). Cell density increased approximately 12-fold from peripheral to central retina from 5 to 60 cells/mm^2. The isodensity contours showed a moderate asymmetry with increased densities extending along the nasotemporal and dorsoventral axes. The cell counts give a mean of 12 cells/mm^2 for the MA ganglion cells. For a retinal area of 450 mm^2 the total number of MA ganglion cells would be 5,400. Given a total number of retinal ganglion cells of ~150,000 (Illing and Wässle, '81) the MA ganglion cells would make up ~3.5% of the total ganglion cell population.

Coverage factor and the dendritic mosaic

Calculation of dendritic coverage factor provided further evidence that the MA ganglion cells constitute a single morphological subpopulation. Estimate of dendritic overlap (mean cell density multiplied by mean dendritic field area) gives an average coverage of 2.2. The coverage factor determined at 2, 4, 8, and 12 mm eccentricity gave values of 1.9, 2.2, 2.2, and 2.4 respectively, indicating that dendritic cover-

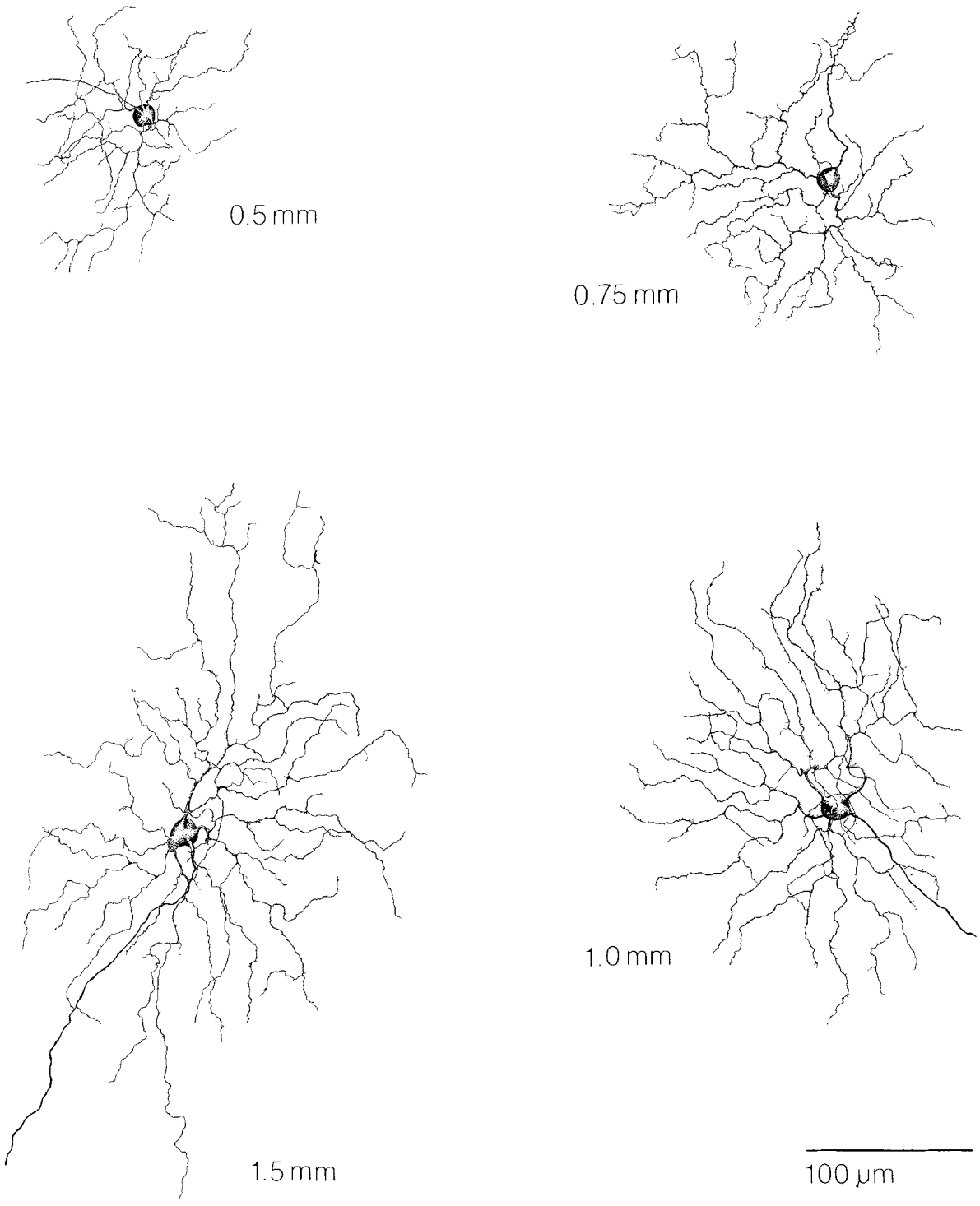

Fig. 4. Variation in dendritic field size and shape of the MA ganglion cells at different retinal eccentricities is illustrated in this Figure and in Figures 5 and 6. Cameral lucida tracings of four cells located within 1.5 mm of the area centralis. Retinal eccentricity in mm is denoted for each cell.

Fig. 5. Camera lucida tracings of MA ganglion cells located in midperipheral retina. Retinal eccentricity in mm is denoted for each cell.

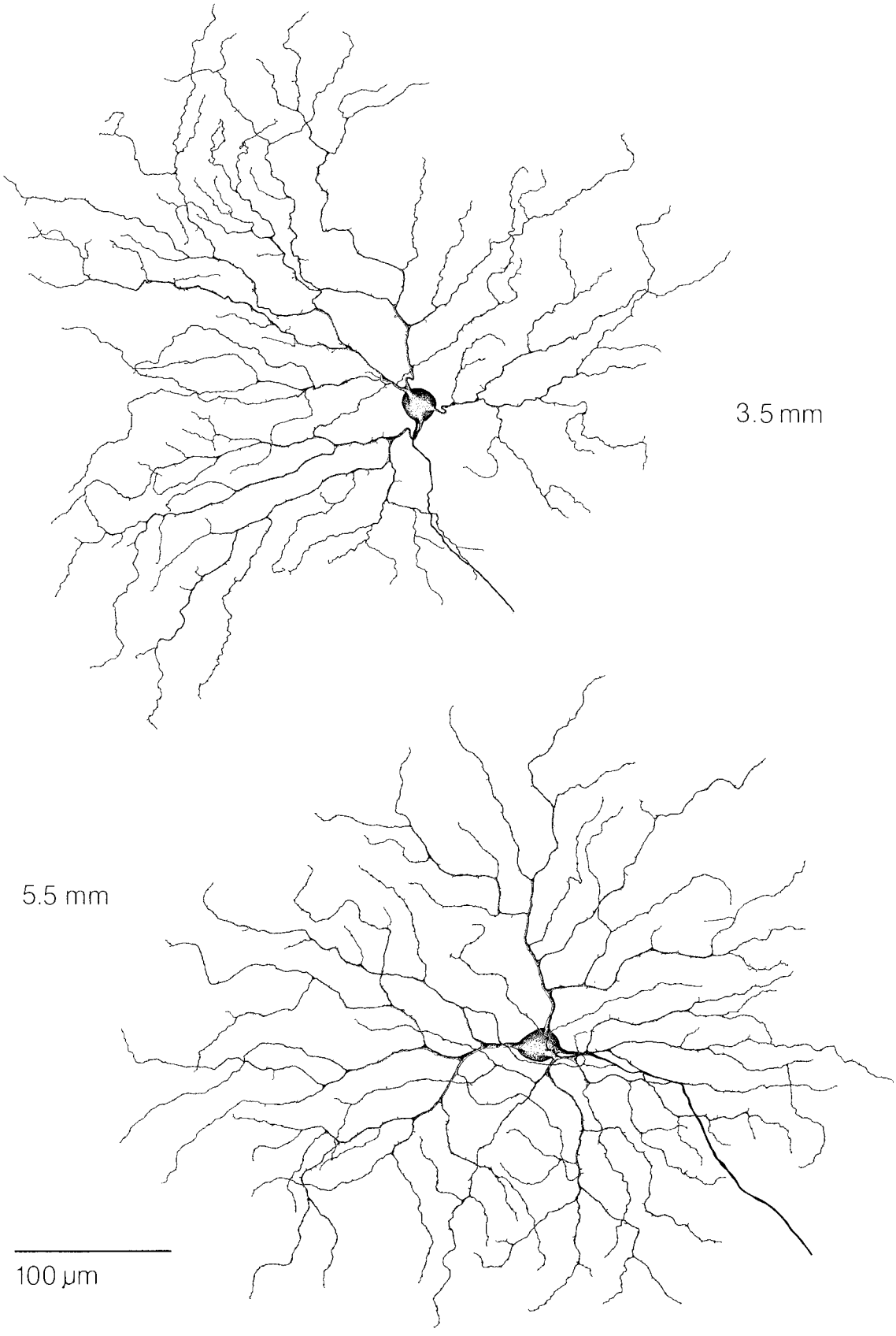

Figure 5

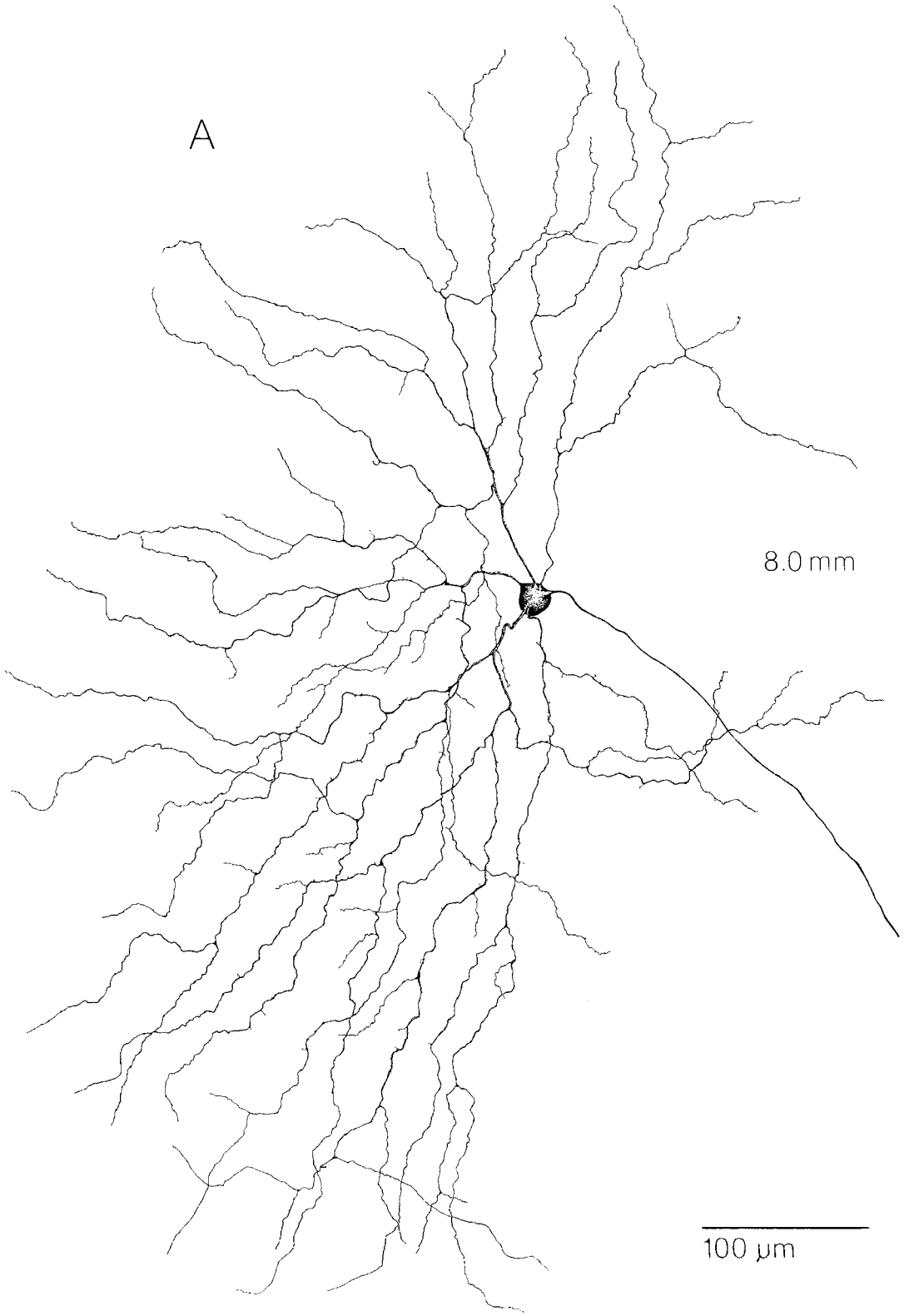

Fig. 6. Camera lucida tracings of MA ganglion cells located in peripheral retina, 8 **(A)** and 13 **(B)** mm from the area centralis. The dendritic field increases in overall size with increasing retinal eccentricity. However, the shape of the dendritic field can vary from roughly circular to a narrow ellipse, and cells at a given eccentricity can differ by about ±25% from the mean dendritic field area for that eccentricity (see also Fig. 8A). The relationship of dendritic branching frequency to dendritic field diameter for a sample of 13 cells whose dendritic trees were completely traced (this sample includes the cells shown in Figs. 3–6 and 15) is shown in the scatterplot in Figure 7.

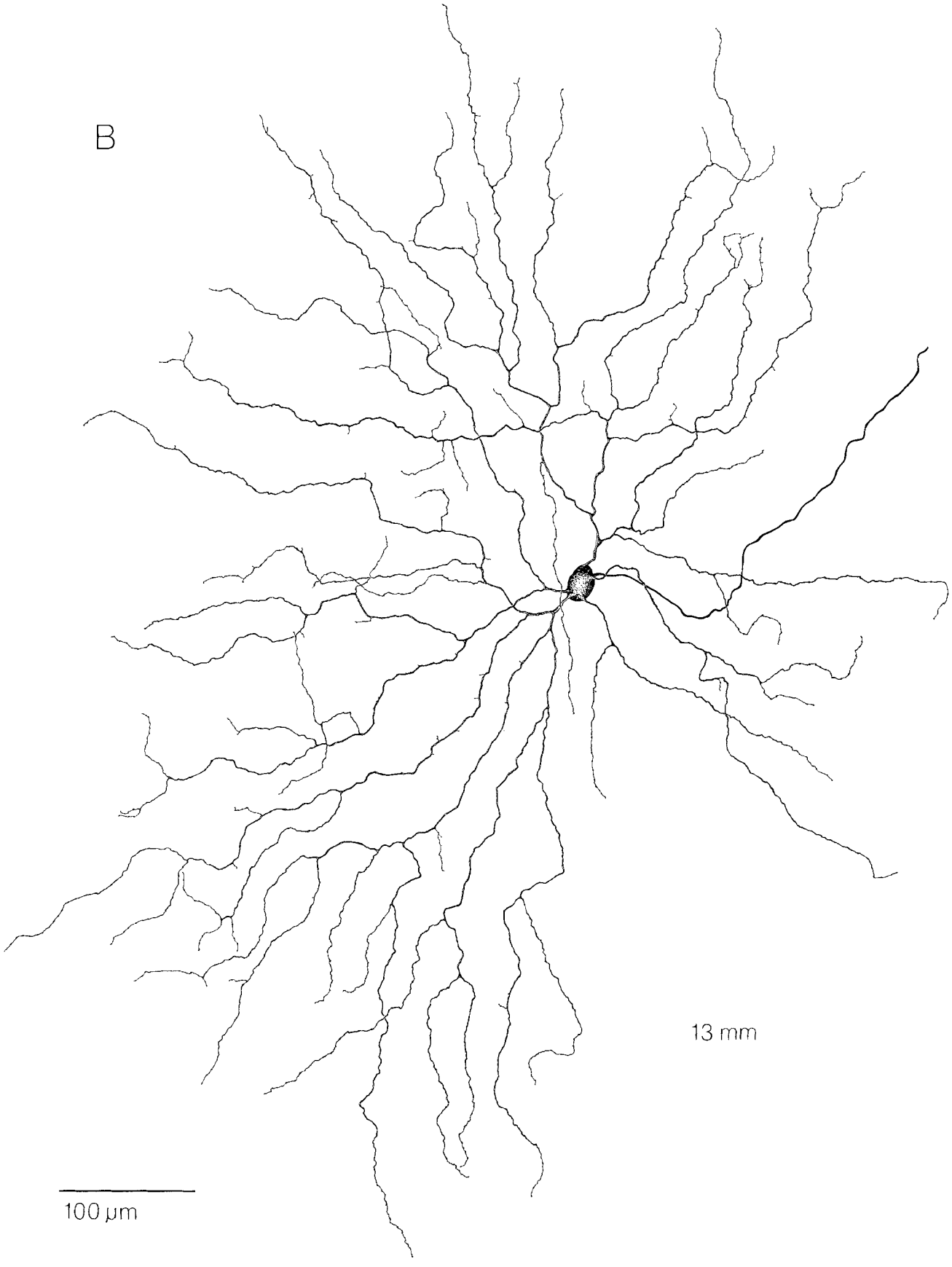

Figure 6 continued

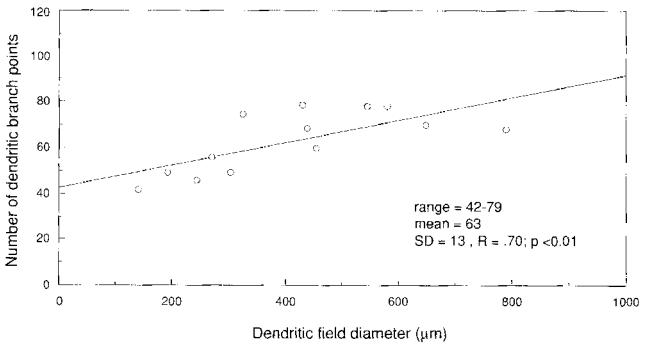

Fig. 7. Scatterplot of number of dendritic branchpoints as a function of dendritic field size for the MA ganglion cell type. A large increase in dendritic field diameter from ~150 to 800 μm is accompanied by a relatively small increase in the total number of dendritic branchpoints. Peripherally located MA ganglion cells thus appear more sparsely branched than centrally located cells because a similar number of dendritic branchpoints is spread over a much larger dendritic field area.

age remains constant from central to peripheral retina. The magnitude of the coverage indicates that, on average, the dendrites of 2–3 cells overlap any given point on the retina. This pattern of dendritic overlap is virtually the same as that shown by Wässle and colleagues for the subpopulations of ON- and OFF-center alpha and beta cells where the dendrites of neighboring cells of the same center sign appear to overlap extensively (Wässle et al., '81a,b).

To directly demonstrate the network of overlapping MA cell dendrites all the fluorescing ganglion cells in a patch of retina were targeted for intracellular injection of HRP. In some instances the dendritic morphology of every or almost every MA cell in the patch was revealed and their dendritic field overlap was directly observed (Fig. 12). The dendrites of 5–7 neighboring cells typically invade the dendritic field of a given cell. (This pattern can be seen clearly in the large, 6 mm patch in Fig. 12.) The soma of a given cell tends to lie at the dendritic field border of its neighbor and individual dendritic branches extend nearly to the center of a neighboring field. A virtually identical pattern of cell body placement and dendritic field overlap has also been observed for the ON- and OFF-center beta cell populations (Wässle et al., '81a).

The extensive dendritic overlap of the MA ganglion cells raises the possibility that, although the cells appear to occupy a single narrow stratum of the IPL, they could compose 2 functionally distinct subpopulations, each with a coverage factor of about 1. Direct observation of the network of overlapping dendrites argues strongly against this possibility. Figure 13 illustrates a camera lucida tracing of the complete dendritic trees of all the cells in the patch located at 5 mm eccentricity in Figure 12. This tracing shows that despite the extensive overlap of the 4 dendritic fields in the upper part of the patch the density of dendritic processes appears to remain constant within the region of overlap. This suggests that the overlap serves to establish a constant local density of dendritic processes despite some degree of variation in cell to cell spacing, and would therefore account for variation in the sizes and shapes of individual dendritic trees. Essentially the same observation was made for the alpha cells where it was observed that the overall dendritic fields appeared to adapt their shapes to fit the available space (Wässle et al., '81b).

A closer look at the nature of the mosaic of overlapping dendrites supports this general hypothesis at the level of individual dendrites. Figure 13 shows that individual dendritic branches of a given cell will often invade the territory of a neighboring cell by extending well beyond the overall elliptical shape of its own dendritic tree. As a consequence many cells have the appearance of projecting a few dendrites well beyond all of the other terminal dendrites. (The cell located at 1.5 mm eccentricity in Fig. 4 illustrates this tendency.) Observations of the patches of injected cells show that these longer dendrites invariably occupy open spaces that exist between the dendritic branches of the neighboring cell. A more common expression of this tendency is that the distal dendritic branches of a cell tend to be more widely spaced than the proximal branches. This pattern can be seen for all of the cells illustrated in Figures 4–6. In this distal half of the dendritic tree neighboring dendrites appear not to intermingle in a random manner but to precisely interdigitate so as to maintain a uniform density of processes and construct a regular interdendritic spacing.

It appears then that there must be a high degree of local order in the positions of individual dendrites within the MA cell plexus. In overlapping dendritic fields, individual dendrites tend to interdigitate rather than cross over one another; the lack of dendritic intersections might thus to be a sensitive measure of the departure from randomness within the plexus. The degree to which the overlapping dendrites deviate from a random placement was therefore evaluated by observing the effect of changing the dendritic tree orientation on the number of dendritic intersections within a local region of overlapping dendrites. This experiment was performed for the dendritic trees of each of the four overlapping cells in the upper part of Figure 13. Each of the 4 cells was rotated from its original orientation by an amount (in degrees) given by a random number sequence. Figure 14A illustrates one such randomized case. The number of points at which dendrites cross over one another (dendritic intersections) were counted in the rectangular area denoted by the arrowheads. This process was repeated seven times and compared with the same dendritic patch in its normal orientation. The results gave a mean ± SD of 181 ± 25 dendritic intersections for the random cases (n = 7; range = 137–218). The number of dendritic intersections for the normal patch was 39. Thus a randomized plexus gave on average 4–5 times the number of intersections than the actual plexus. The manner in which the random rotations altered the plexus can be appreciated by the intersection plots illustrated in Figure 14B. The number and location of dendritic intersections for the actual plexus (Fig. 13) and for two of the random cases are shown within the rectangles. Any change in the relative placement of the dendritic branches results in a dramatic increase in the number of dendritic intersections. This resulted principally from dendrites clustering together and crossing over many times within a small region, a feature that was never observed in the normally oriented patches.

DISCUSSION

The MA ganglion cells are an identifiable subpopulation that can be distinguished morphologically from the previously characterized alpha and beta ganglion cell types (Fig. 15; Table 1). In Figure 15 some of these differences can be seen by comparing examples of an HRP-filled outer-alpha cell, an outer-beta cell, and an MA cell from about 1 mm ret-

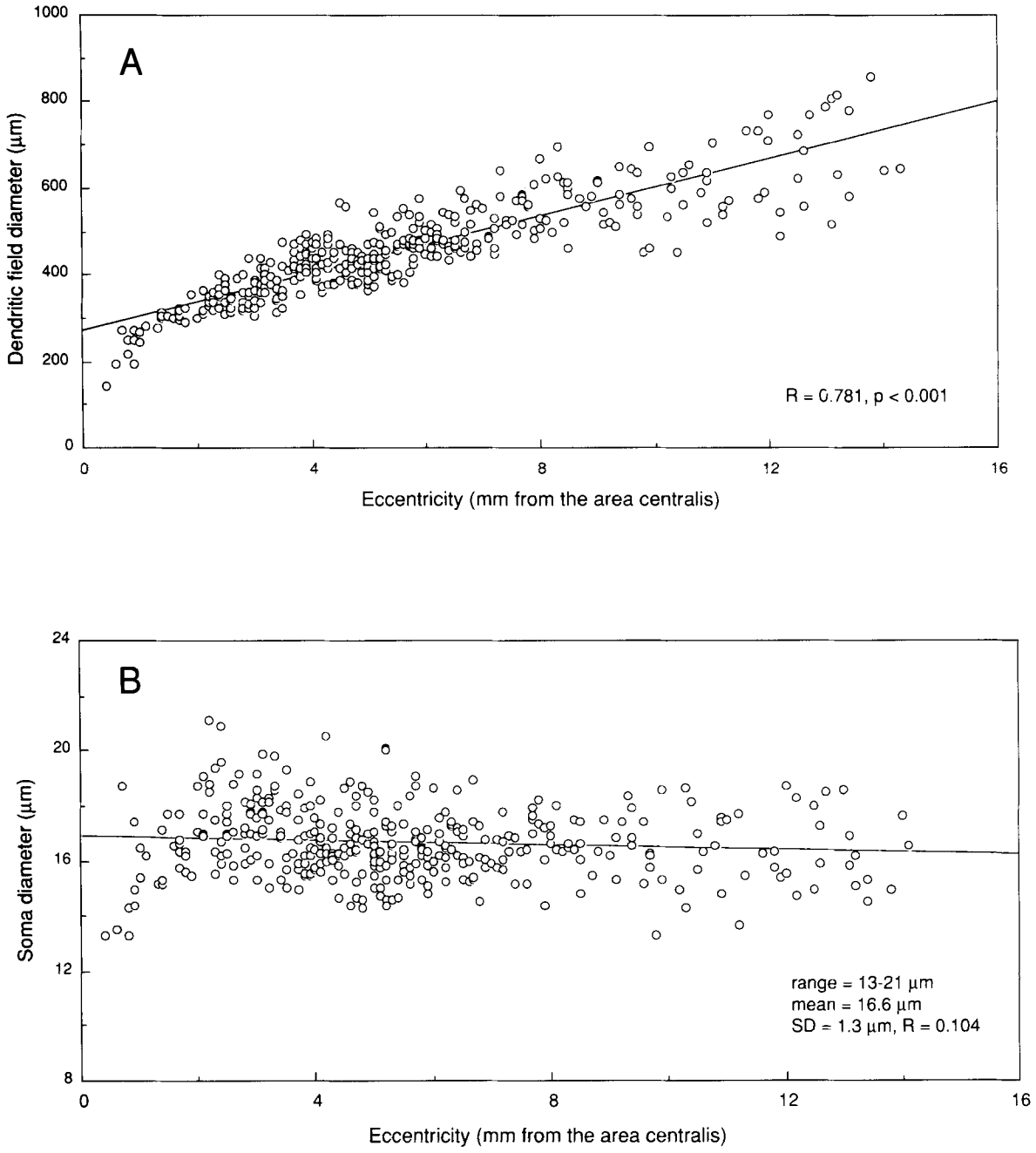

Fig. 8. Scatterplot of dendritic field diameter (**A**) and soma diameter (**B**) as a function of retinal eccentricity for the MA ganglion cell type. Dendritic field size increases from ~150–200 μm in diameter at 0.5 mm eccentricity to ~600–800 μm in diameter at 14 mm eccentricity. Dendritic field size and eccentricity show a significant positive correlation ($R = 0.78$, $P < 0.001$). Soma size ranged from 13–21 μm in diameter (mean = 16.6 μm; SD = 1.3 μm). No correlation of soma size with retinal eccentricity was evident. Slight distortions in soma size resulting from electrode penetration (as discussed in the results) are likely to be a source of artifactual variation in soma size.

inal eccentricity. The MA cell has only a slightly smaller dendritic field size than the alpha cell, despite its much smaller soma size (see Fig. 9A also). Both cell types show a similar, narrowly stratified branching pattern marked by very little crossing over of individual dendrites. At all branch orders, however, the dendrites of the MA cell appear much thinner than those of the alpha cell. Both the MA and the alpha cell contrast with the smaller, more highly branched, and broadly stratified beta cell.

The MA cells are almost certainly equivalent to at least a subset of the indoleamine-accumulating ganglion cells recently identified in the cat's retina (Wässle et al., '87). In that study, formaldehyde-induced histofluorescence was promoted by uptake of 5,7-DHT and a ganglion cell popula-

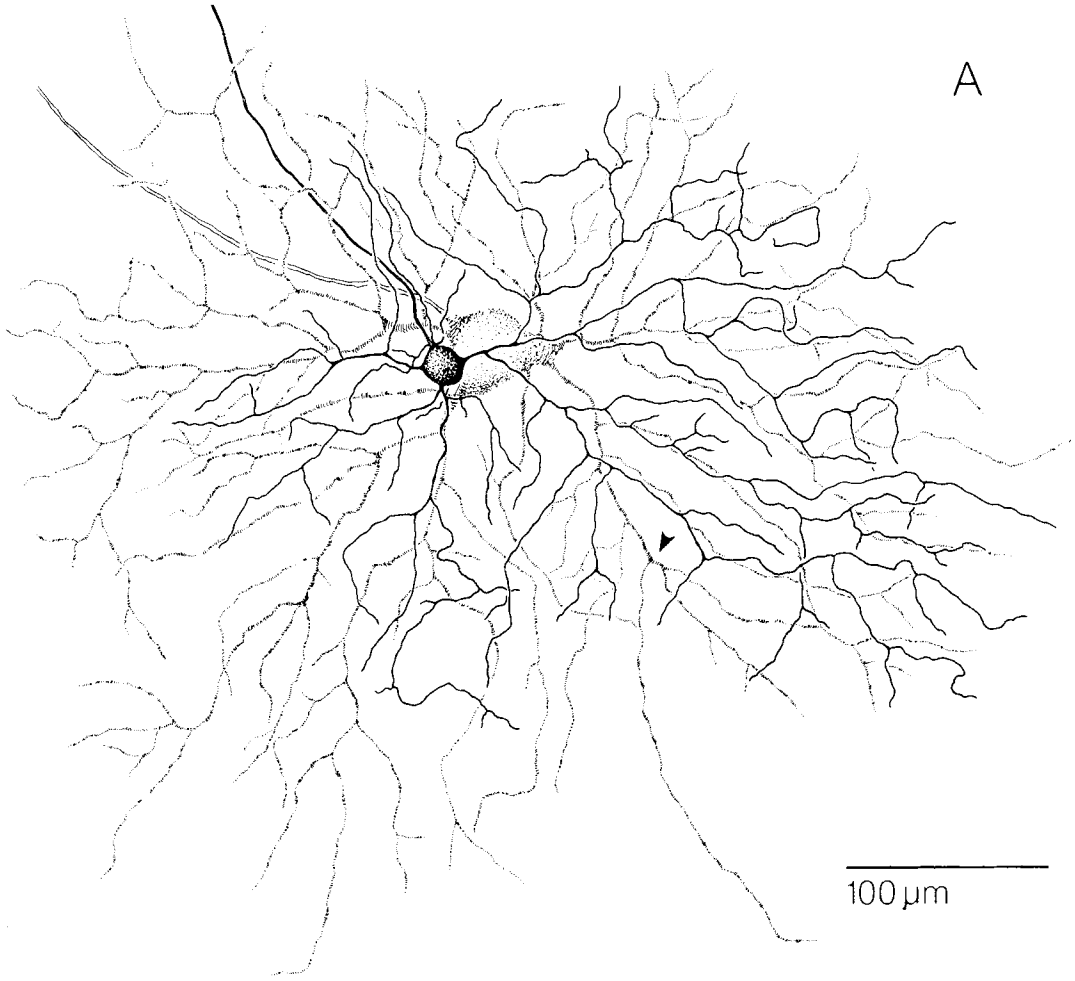

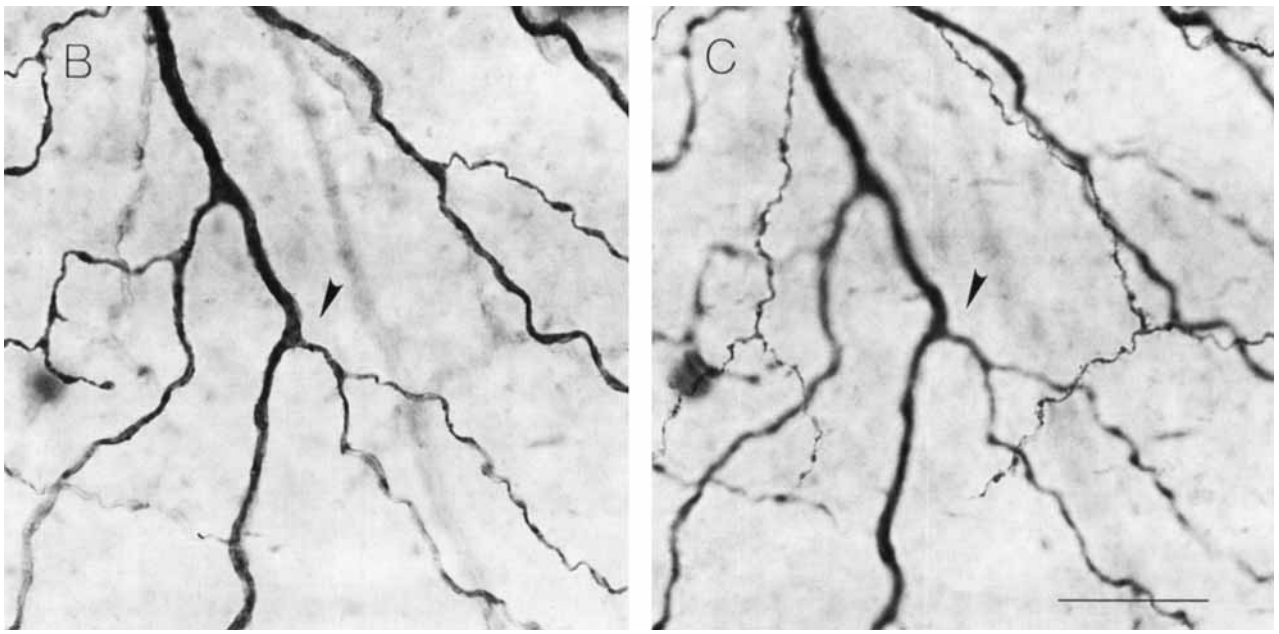

Fig. 9. Depth of stratification of the MA ganglion cell dendritic tree and a comparison with the outer-alpha cell. **A:** Camera lucida tracings of intracellularly injected MA ganglion cell (shown by the solid tracing) and a neighboring outer-alpha cell (shown by the light stippling) with highly overlapped dendritic trees. Measurements of the relative depth of stratification for the 2 cells are shown in the histogram in Figure 10B. **B** and **C:** Photomicrographs of a part of the overlapping dendritic trees of the alpha and MA cell. In **B** the plane of focus is on the thick alpha cell dendrites and in **C** the plane of focus is on the much thinner MA cell dendrites. MA ganglion cell stratification is situated closer to the inner nuclear layer border than the outer-alpha cell. The same location in panels A–C is indicated by the arrowheads.

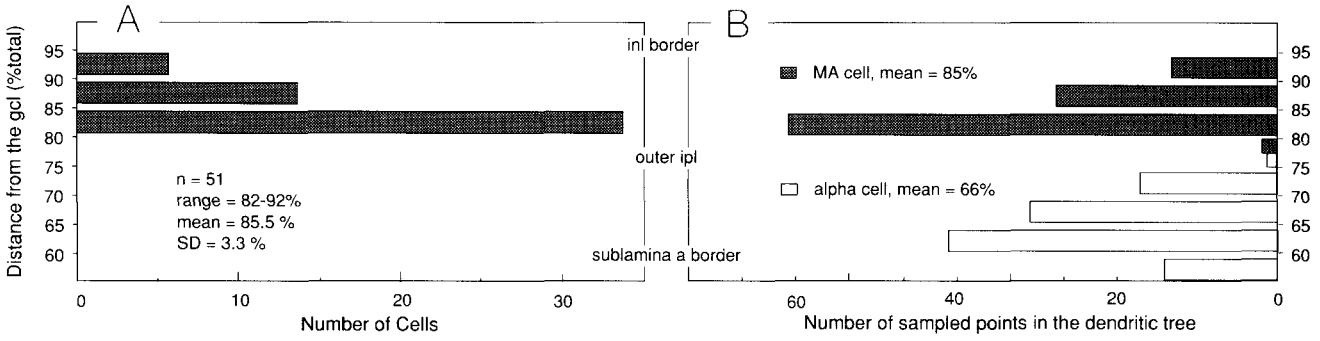

Fig. 10. The relative depth of the dendritic tree of the MA and alpha cell as a percentage of the total thickness of the inner plexiform layer. **A:** This histogram shows the depth of stratification for a sample of 51 HRP-filled MA cells. In this data one measurement was taken for the depth of the dendritic tree for each of the cells in the sample. **B:** This histogram gives the relative depth of stratification for the single outer-alpha and MA cell illustrated in Figure 9. Depth readings were taken for each cell at 99 points where individual dendrites of the two cells crossed over one another.

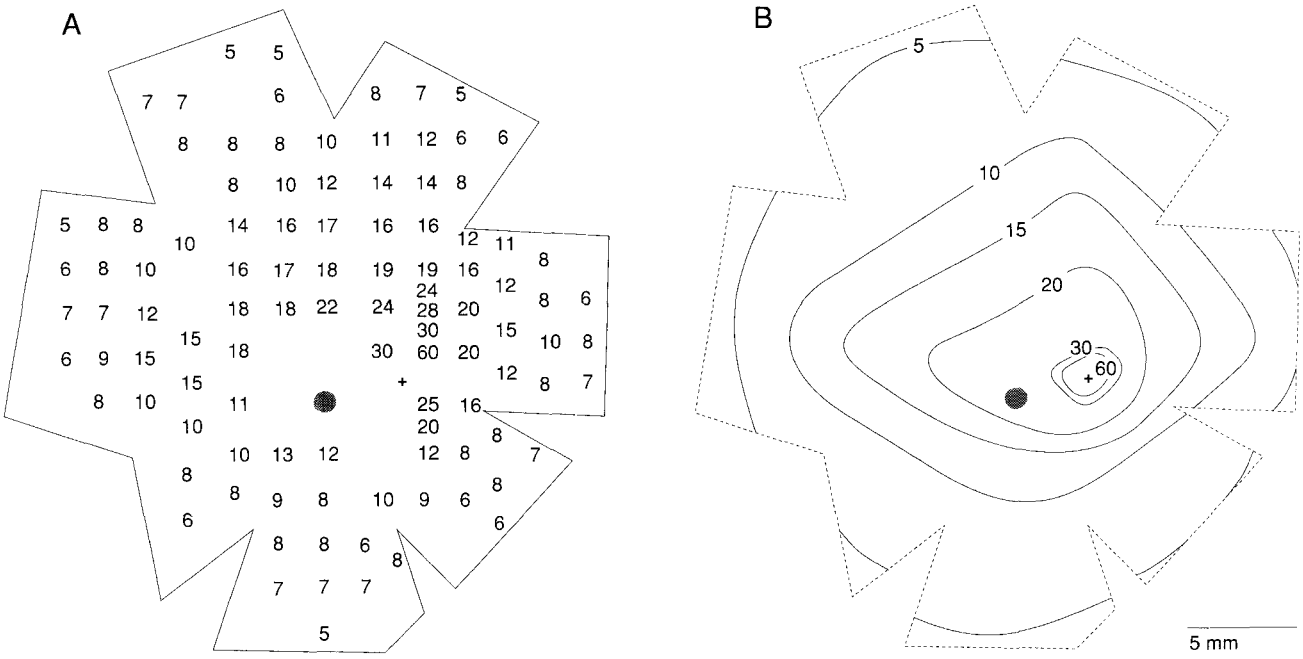

Fig. 11. Topography of the MA ganglion cell population. **A:** A map of a cat retinal wholemount that shows counts of fluorescing MA ganglion cells made at 104 locations in the in vitro retina. Counts were made over a 0.5× 1 mm area. The counts shown have been multiplied by 2 to give cells/mm^2. **B:** Isodensity map generated from the counts shown in A. The measured density of MA cells ranges from 5 cells/mm^2 in the far retinal periphery to 60 cells/mm^2 within 1 mm from the area centralis. Isodensity contour lines were fitted by eye. The density distribution is not symmetrical around the area centralis but is slightly cruciform with increased density extended along the nasotemporal and dorsoventral axes.

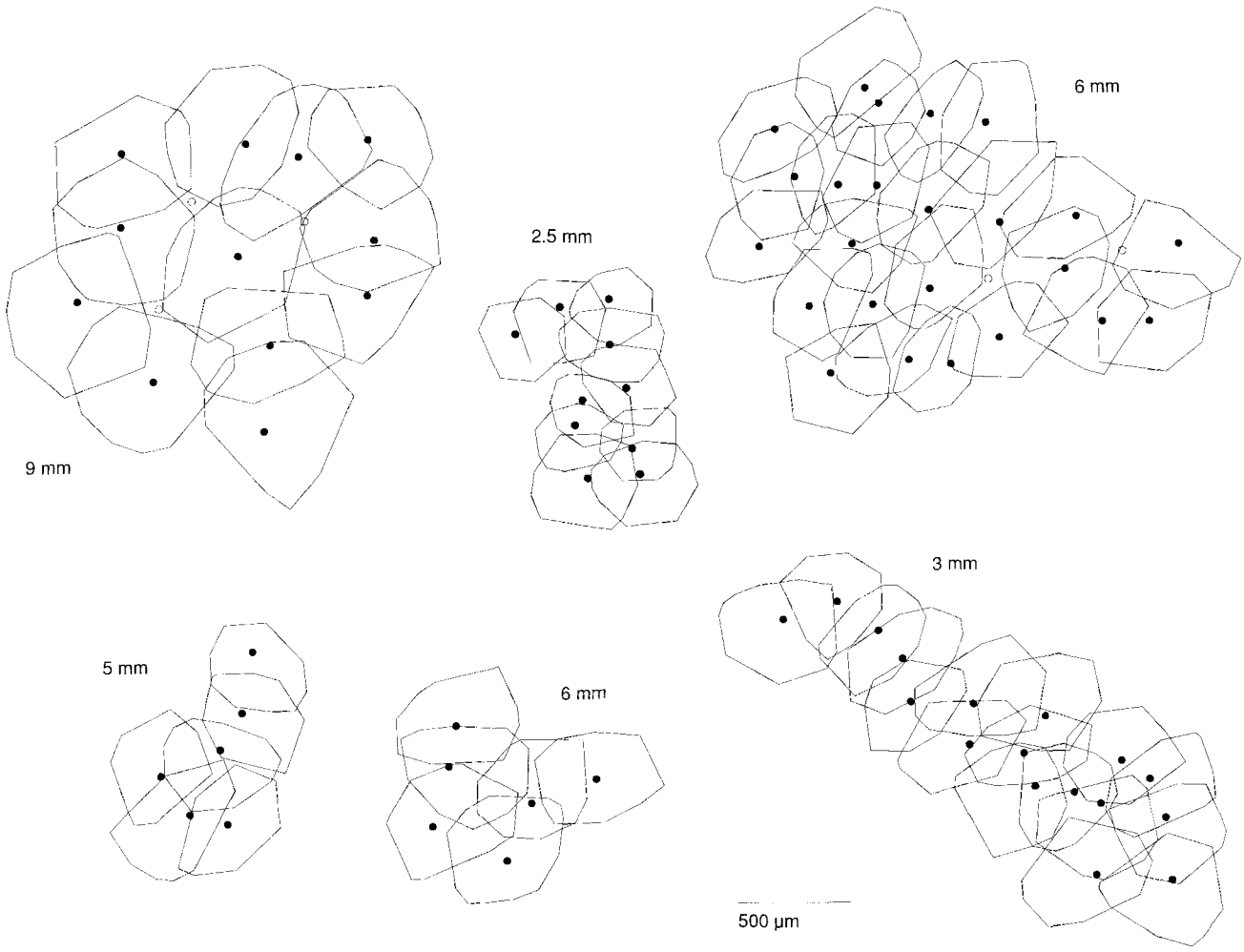

Fig. 12. Mosaic organization of the MA cell dendritic fields. To observe the overlapping dendritic fields of the MA ganglion cells every fluorescing ganglion cell in a patch of retina was injected with HRP. Several patches in which all or most cells were successfully filled with HRP are shown here. The location of each injected soma is marked by the small filled circles. The extent of the dendritic tree for each cell is denoted by tracing a convex polygon around the extremities of the dendrites. Retinal eccentricity in mm is also given for each patch. The location of cell bodies whose dendritic trees were not filled well enough to accurately determine dendritic field size are marked by the open circles in the 9 mm and 6 mm patches.

tion was identified by injecting Lucifer yellow into fluorescing cells following the protocol of Tauchi and Masland ('84) for intracellular staining in fixed tissue. Twelve successfully injected cells resembled in size and dendritic morphology the cells described in the present paper. The depth of stratification of these cells was not given but it was noted that injected cells appeared to stratify in either the inner-ON or outer-OFF sublaminae of the inner plexiform layer, and it was therefore suggested that two morphologically similar cell types, an ON- and OFF-center pair, composed the fluorescing ganglion cell subpopulation. The present study found no evidence for a monoamine-accumulating cell that stratified in the inner-ON sublamina; all of the 374 cells analysed were narrowly stratified at the outer border of the inner plexiform layer, within the outer-OFF-sublamina.

The uptake of dopamine and 5,7-DHT by a ganglion cell population suggests that a monoamine may serve as a ganglion cell neurotransmitter. However, immunohistochemical demonstration of tyrosine hydroxylase, the rate-limiting enzyme in the biosynthesis of dopamine, as well as formaldehyde-induced catecholamine histofluorescence, have only been consistently observed in amacrine cell populations in the mammalian retina (e.g., Törk and Stone, '80; Oyster et al., '85). Similarly, serotonin has not been detected in the mammalian retina by immunohistochemistry and levels of endogenous serotonin are very low (Osborne et al., '82; Tornqvist et al., '83). Despite these negative findings evidence from other species suggest that the presence of a monoaminergic ganglion cell type in the cat's retina should not be discounted. Tyrosine-hydroxylase-immunoreactive ganglion cells have been occasionally observed in the ferret retina with a size and stratification similar to the cat MA ganglion cell (H. Karten, personal communication). Two distinct subpopulations of tyrosine-hydroxylase-immunore-

active ganglion cells have recently been identified in the pigeon's retina; one population is displaced to the inner nuclear layer and projects to the accessory optic nucleus (Britto et al., '88) and the other is located in the ganglion cell layer and projects to the optic tectum (Keyser et al., '87). A serotonin-immunoreactive ganglion cell type has also been identified in the turtle's retina (Weiler and Ammermüller, '86).

If a monoamine does serve as a mammalian ganglion cell transmitter, but simply is present at levels too low to be detected in the soma or dendrites, then it might be more easily detected where the transmitter is released, in ganglion cell axon terminals. Is there any evidence for disproportionately high levels of monoamines in retinal target structures? Immunohistochemical demonstration of serotoninergic axons in cats, rats, and monkeys does reveal striking variation in terminal density within the subdivisions of the visual thalamus (Ueda and Sano, '86; De Lima and Singer, '87). In all 3 animals the ventral lateral geniculate receives a much greater input than the dorsal lateral geniculate nucleus. Within the dorsal lateral geniculate complex of the cat, the C-laminae and the medial interlaminar nucleus receive a conspicuously greater serotoninergic input than the A-laminae. Similarly, the S layer and the interlaminar zones of the macaque lateral geniculate nucleus also receive a much greater input than the magno- and parvicellular layers. A dense serotoninergic input to the superficial, retinorecipient layers of the superior colliculus has also been observed (Ueda et al., '85). As noted by Ueda and Sano, the regions that receive a particularly dense 5-HT projection correspond to targets of retinal W cells, that is, ganglion cell types other than the X and Y cells. Thus, although direct evidence is required, the possibility exists that some percentage of the serotoninergic input to the ventral and dorsal lateral geniculate and the superior colliculus may derive from a monoaminergic retinal ganglion cell type.

The monoamine-accumulating ganglion cell appears to have been observed consistently in previous morphological studies of cat retinal ganglion cells. In Golgi preparations Boycott and Wässle ('74) observed a special category of gamma cell that they called the delta cell. The delta cells (n = 11) showed a soma size (~15–20 μm), a dendritic field size range (from ~250 μm at 1 mm eccentricity to ~600 μm at 12 mm eccentricity), and a dendritic branching pattern similar to the MA ganglion cell (e.g., Boycott and Wässle, '74, their Fig. 5C). Cells with a similar morphology were subsequently observed and called medium soma gamma cells (Stone and Clarke, '80) and G18 or G19 (Kolb et al., '81). Cells with this morphology were also observed after extracellular injections of HRP made directly into the retina and were termed Class 4 cells (Dacey, '84).

Several studies have attempted to correlate receptive field properties with ganglion cell dendritic morphology beyond the alpha-Y and beta-X cells. In total, the morphology of 22 physiologically characterized ganglion cells, that were neither Y-alpha nor X-beta cells, has been observed following intracellular injection of HRP or Lucifer yellow in 3 independent studies (Saito, '83—2 cells; Fukuda et al., '84—4 cells; Stanford, '86—16 cells). Eleven cells fell into the sluggish-sustained category, and the remainder included a number of types with transient responses to light stimulation or a lack of clear center-surround organization. In general, the more frequently encountered sluggish-sustained cells showed larger soma sizes and faster axonal conduction velocities than the less frequently encountered types. Due to the small sample size the dendritic morphology of the sluggish-sustained cells could not be studied in detail in the above studies. However, it did appear that the 11 sluggish-sustained cells formed a morphologically similar group comparable in size and branching pattern to the MA ganglion cells of the present study and the delta cells of previous Golgi studies. (For a clear example compare the OFF-center tonic W-cell shown in Figure 4C of Stanford, '86, with the MA cells.) By contrast, the other physiological types appeared to include cells that, when compared to the MA cells, showed dendritic trees that were either larger and more sparsely branched, or smaller and more densely branched. The existing evidence thus suggests that the MA ganglion cells may correspond to the concentrically organized, sluggish-sustained physiological type according to the terminology developed by Cleland and Levick, ('74a,b). This physiological type is also referred to as the tonic-W cell (Stone and Fukuda, '74) and as the Q cell (Enroth-Cugell et al., '83).

The stratification of the MA cells suggests that they will be of the OFF type, but sluggish-sustained cells have been divided into both ON- and OFF-center types that have been typically isolated with equal frequency by the recording electrode (for an exception see Enroth-Cugell et al., '83). This would predict the existence of a cell type morphologically similar to the MA cell but that stratifies in the ON-sublamina of the inner plexiform layer. Two examples of HRP-filled ON-center sluggish-sustained cells (Stanford, '86, Fig. 4A,D of that paper) are similar in soma size and dendritic field size of identified OFF-center sluggish-sustained cells but appear to be more sparsely branched. A possible parallel can be found in the alpha cells where the inner and outer types also differ significantly in number of dendritic branches (Dacey, '85).

There is evidence that the MA ganglion cells project to the superior colliculus and/or the dorsal lateral geniculate nucleus. Cells of the appropriate soma size have been retrogradely labeled from both structures (Wässle and Illing, '80; Illing and Wässle, '81). Injections of rhodamine-labeled microspheres into the superior colliculus and the C-laminae of the dorsal lateral geniculate nucleus have recently been used to target retrogradely labeled ganglion cells for intracellular injection of HRP under direct microscopic control in an in vitro retinal preparation (Brening and Rodieck, '86; Rodieck and Watanabe, '86). These studies demonstrated that a number of morphologically distinct ganglion cell types project to each structure. Cells comparable in dendritic morphology and size to the MA cells were retrogradely labeled from both the C-laminae and the superior colliculus. By contrast the subset of ganglion cells (the epsilon cells) that project to the geniculate wing can be distinguished from the MA cells by a larger soma and dendritic field and a more sparsely branching dendritic tree (Leventhal et al., '80; Rodieck and Watanabe, '86). Ganglion cell projections to the medial terminal nucleus of the accessory-optic system (Farmer and Rodieck, '82; Rodieck, personal communication; Buhl and Peichl, '86; Dann and Buhl, '87) also derive from cells that are morphologically distinct from the MA cells.

The evidence that the monoamine-accumulating ganglion cells correspond to sluggish-sustained cells and project to the superior colliculus and/or the C-laminae of the dorsal lateral geniculate nucleus is consistent with antidromic activation and conduction latency studies of the central projections of the different receptive field types of ganglion cells. All ganglion cell types with the possible exception of X-beta

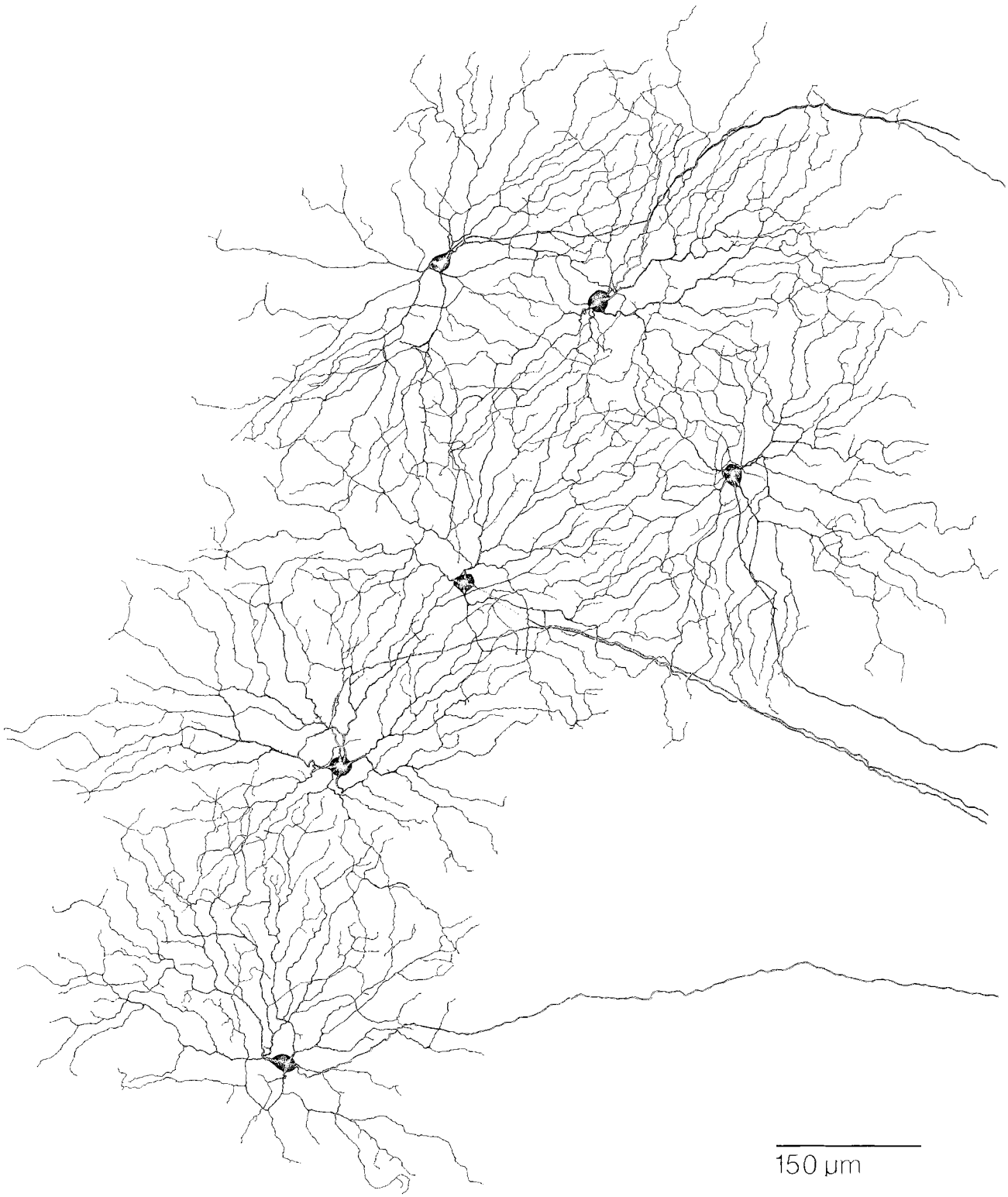

Fig. 13. The MA ganglion cell dendritic plexus. A camera lucida tracing of all of the cells in one patch of 6 cells (5 mm eccentricity) shown in Figure 12 illustrates the organization of the plexus created by the overlapping dendritic fields. The density of dendrites appears to remain constant across the core of patch where the processes of 4 cells intermingle and overlap extensively. Individual dendritic branches also appear to show a high degree of local order by interdigitating to fill available space within the network. The degree to which the interdigitating dendrites deviate from a random orientation is estimated in Figure 14.

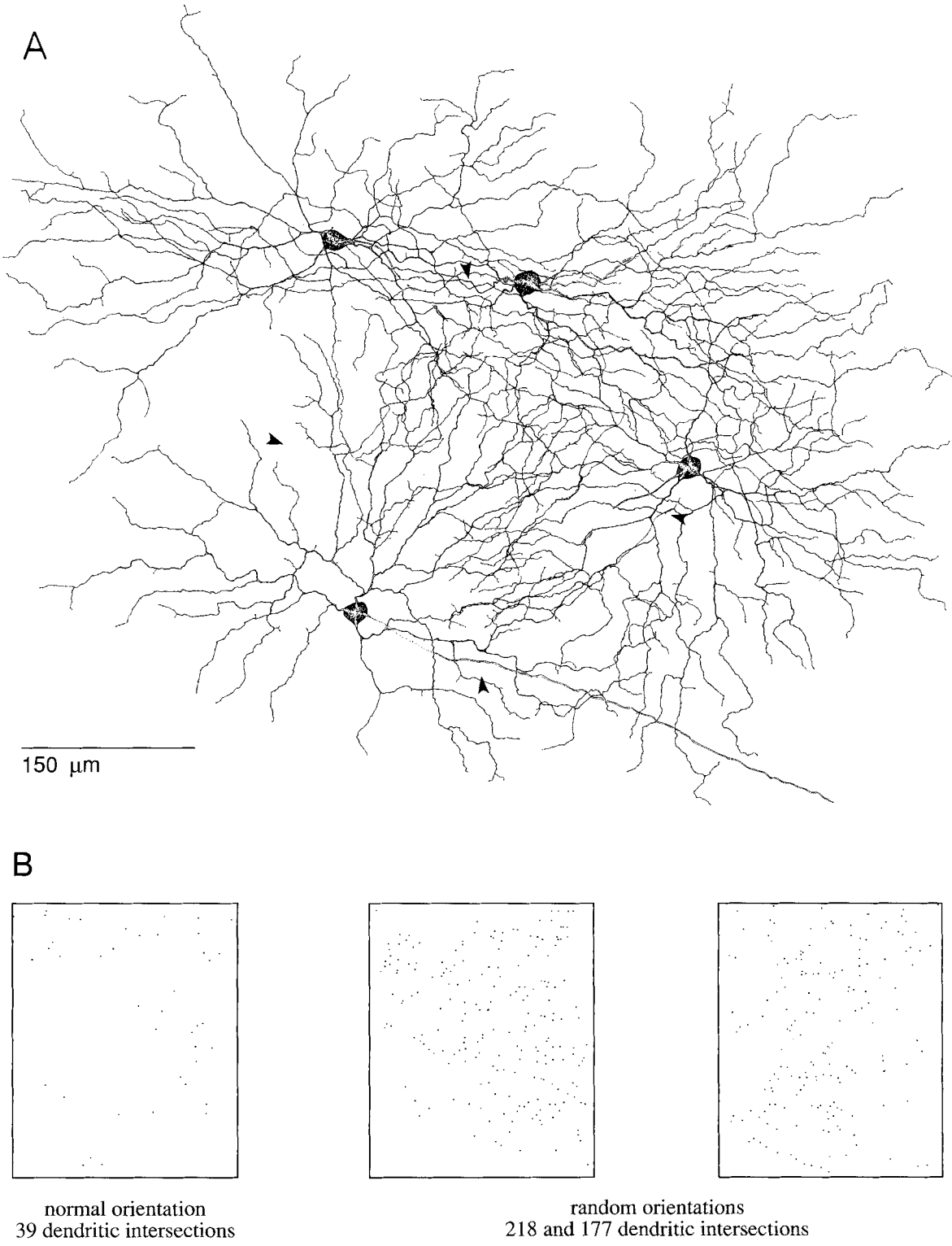

Fig. 14. Evidence for a high degree of local order in the positions of individual dendrites within the MA cell plexus. **A:** The upper 4 cells in the patch illustrated in Figure 13 are shown here after the orientation of the dendritic trees was randomized by rotating each dendritic tree by an amount (in degrees) given by a random number sequence. The number of points at which dendrites crossed over one another (dendritic intersections) was counted within the rectangle denoted by the arrowheads. This process was repeated with 7 different random number sequences. The results gave a mean ± SD of 181 ± 25 dendritic intersections for the random cases (n = 7; range = 137–218). By contrast the number of intersections for the dendrites at their normal orientation (shown in Fig. 13) is 39. Thus a randomized plexus gave on average 4–5 times the number of intersections as the actual plexus. **B:** The rectangles show the number and location of dendritic intersections (marked by the points) for the actual plexus (Fig. 13) and for 2 of the random cases.

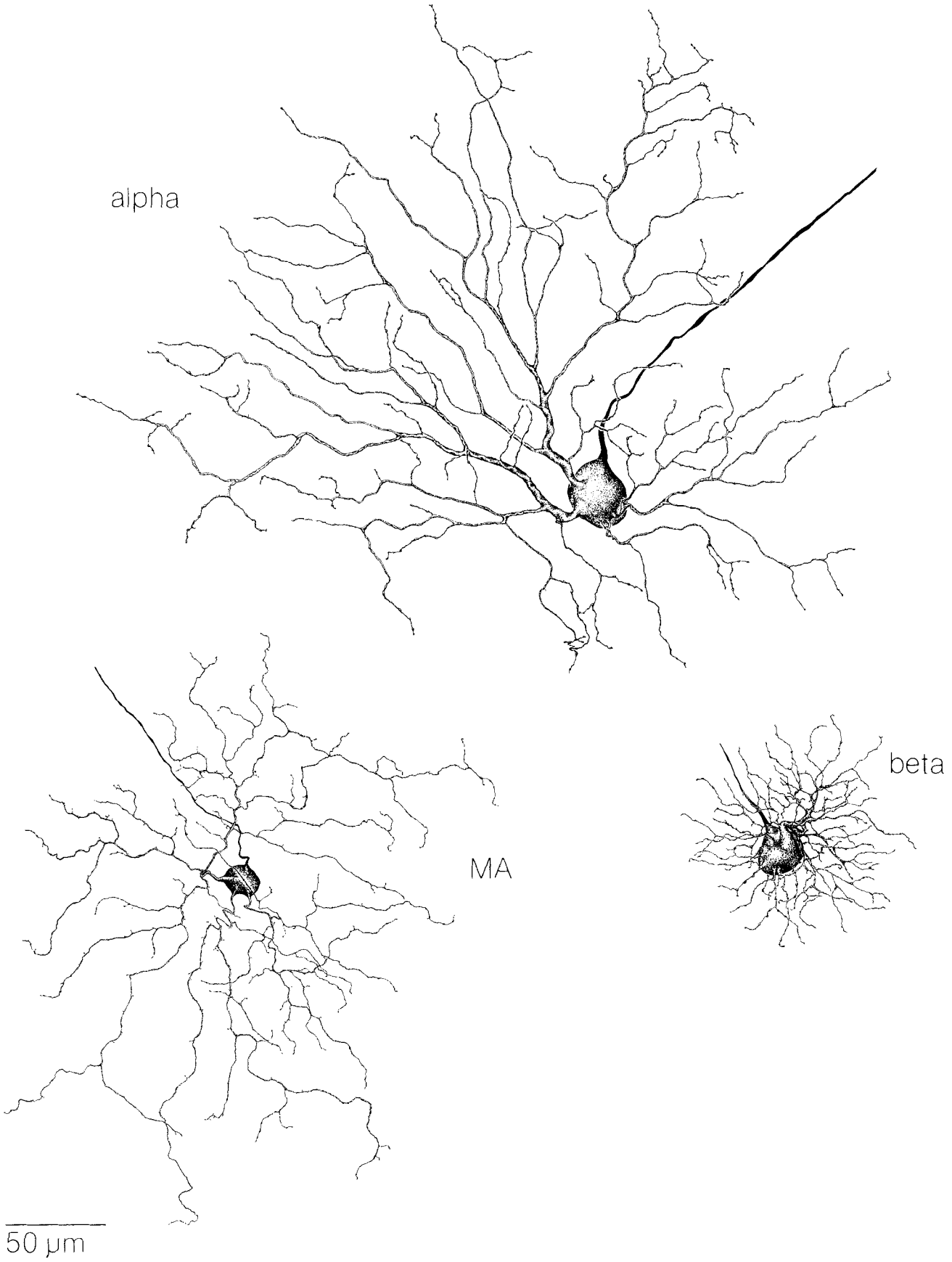

Figure 15

TABLE 1. Comparison of 3 Types of Cat Retinal Ganglion Cells That Stratify in Sublamina a of the Inner Plexiform Layer[1]

	Outer-alpha cell	Outer-beta cell	MA cell
Soma diameter (μm)	17–35	13–24	13–21
Dendritic field diameter (μm)	180–1,000	25–300	150–800
Dendritic stratification	S2	S1–2	S1
Coverage factor	1.7	3.1	2.2
Proportion of total population (%)	2	25–30	3.5
Receptive field type	OFF center, brisk-transient (Y)	OFF-center, brisk-sustained (X)	OFF-center? sluggish-sustained?
Central projections	A & C laminae DLGN, MIN, SC	A laminae DLGN	C-laminae DLGN? VLGN, SC?

[1]The division of the inner plexiform layer into sublamina a and b and strata 1–5 follows Famiglietti and Kolb ('76). Morphological data for the outer alpha and beta cells follows Wässle et al. ('81a,b) (dendritic field size, soma size, and coverage factor), McGuire et al. ('86), Freed and Sterling ('88), Wässle et al. ('81a,b) (stratification), and Illing and Wässle ('81) (proportion of total population). The use of outer beta and outer alpha to denote the morphology of the OFF-center X and Y cells follows Wässle et al. ('81a,b). The receptive field type and central projections for the MA ganglion cell type are hypotheses based on evidence considered in the discussion. Abbreviations: DLGN—dorsal lateral geniculate nucleus; MIN—medial interlaminar nucleus; SC—superior colliculus; VLGN—ventral lateral geniculate nucleus.

cells have been antidromically activated from the superior colliculus (Cleland and Levick, '74a,b; Fukuda and Stone, '74). The dense, crossed projection to the upper layer of the retinal recipient zone consists of principally extremely slow-conducting axons that are likely to derive from sluggish-transient and certain nonconcentrically organized types (Berson, '87). It has been suggested therefore that the sluggish-sustained cells provide a faster-conducting, bilateral projection to the middle layer of the retinal recipient zone (see Berson, '87, for review). Similarly, orthodromic latency and receptive field analysis of neurons in the dorsal lateral geniculate nucleus suggest that the sluggish-sustained ganglion cells project principally to the C-laminae (e.g., Wilson et al., '76; Cleland et al., '76; Sur and Sherman, '82).

Observations of the dendritic network formed by the mosaic of overlapping dendritic fields for the monoamine-accumulating ganglion cell type show that despite the relatively high degree of dendritic field overlap a single, locally ordered network is created. It is possible, given the average coverage factor of 2.2, that the MA cells consist of two independent mosaics that each could completely tile the retina as is the case for the ON- and OFF-center alpha-Y cells (Wässle et al., '81b). The injection of every fluorescing MA ganglion cell in discrete patches of retina reveals that this is not the case. The overlapping dendritic fields occupy a single strata and produce a qualitatively uniform density that is constructed by an orderly interdigitation of the individual dendritic branches of overlapping cells (Fig. 13). The spatial arrangement of individual dendrites appears to be very precise. Rotating the dendritic fields within the network by a random amount results in a striking increase in the number of dendritic intersections (Fig. 14). Thus there appears to be an active mechanism that determines the spatial relationships among individual neighboring dendrites within the plexus.

The functional significance of the orderly arrangement of neighboring dendrites is likely to reside in their synaptic relations with other cell types. Local order in a dendritic network has also been observed for the population of cholinergic amacrine cells (Tauchi and Masland, '85). Light and electron microscopic analysis of cholinergic dendrites in rabbit suggest that they are spatially linked to a network of similar dimension formed by postsynaptic dendrites of a bistratified, direction-selective ganglion cell type (Brandon, '87; Vaney et al., '88). In the cat's retina the network of cholinergic processes may be similarly related to the dendrites of alpha ganglion cells (Vardi et al., '88). A variety of amacrine cell types, including the large, dopaminergic amacrine, stratify exclusively at the outer border of the inner plexiform layer. It remains to be determined if any of these form a specific synaptic relationship with the MA ganglion cell type.

Fig. 15. Comparison of the dendritic morphology of the MA ganglion cell type with the outer-alpha cell and the outer-beta cell of the cat's retina. The dendritic trees of the outer-alpha and the MA cell are narrowly stratified in distinct portions of sublamina a and show few overlapping dendrites. By contrast the more bushy-appearing beta cell is broadly stratified over a large extent of sublamina a and thus shows many overlapping dendrites when observed in a wholemount preparation. The individual dendrites of the MA cell are also thinner than those of either the alpha or beta cell (see also Fig. 7B,C). Retinal eccentricity for all 3 cells shown is approximately 1.0 mm from the area centralis. A further comparison of some of the properties of these 3 cell types is given in Table 1.

ACKNOWLEDGMENTS

This work was supported by NIH grant EY06678. I thank R.W. Rodieck for helpful discussions and for providing the space required to gather the data for this study. D. Berson, H. van Brederode, C. Curcio, M. Koontz, K. Mulligan, and H. Sherk offered helpful comments on the manuscript. Technical assistance was provided by M. Clarke, T. Haun, and W. Gardiner.

LITERATURE CITED

Ames, A., and F.B. Nesbett (1981) In vitro retina as an experimental model of the central nervous system. J. Neurochem. *37*:867–877.

Berson, D.M. (1987) Retinal W-cell input to the upper superficial layer of the cat's superior colliculus: A conduction velocity analysis. J. Neurophysiol. *58*:1035–1051.

Boycott, B.B., and H. Wässle (1974) The morphological types of ganglion cells of the domestic cat's retina. J. Physiol. (Lond.) *240*:397–419.

Brandon, C. (1987) Cholinergic neurons in the rabbit retina: Dendritic branching and ultrastructural connectivity. Brain Res. *426*:119–130.

Brening, R.K., and R.W. Rodieck (1986) Morphology of cat ganglion cells that project to the superior colliculus. Invest. Ophthalmol. Vis. Sci. [Suppl.] *27*:223.

Britto, L.R.G., K.T. Keyser, D.E. Hamassaki, and H.J. Karten (1988) Catecholaminergic subpopulation of retinal displaced ganglion cells projects to the accessory optic nucleus in the pigeon (*Columbia livia*). J. Comp. Neurol. *269*:109–117.

Brown, K.T., and D.G. Flaming (1986) Advanced Micropipette Techniques for Cell Physiology. IBRO handbook series: Methods in the Neurosciences, 9. Great Britain: John Wiley & Sons.

Buhl, E.H., and L. Peichl (1986) Morphology of rabbit retinal ganglion cells projecting to the medial terminal nucleus of the accessory optic system. J. Comp. Neurol. *253*:163–174.

Cleland, B.G., and W.R. Levick (1974a) Brisk and sluggish concentrically organized ganglion cells of the cat's retina. J. Physiol. (Lond.) *240*:421–456.

Cleland, B.G., and W.R. Levick (1974b) Properties of rarely encountered

types of ganglion cells in the cat's retina and an overall classification. J. Physiol. (Lond.) *240*:457–492.

Cleland, B.G., W.R. Levick, R. Morstyn and H.G. Wagner (1976) Lateral geniculate relay of slowly conducting retinal afferents to cat visual cortex. J. Physiol. 255:299–320.

Dacey, D. (1984) Light microscopy of HRP-filled cat retinal ganglion cells. Neurosci. Abstr. *10*:838.

Dacey, D.M. (1985a) Wide-spreading terminal axons in the inner plexiform layer of the cat's retina: Evidence for intrinsic axon collaterals of ganglion cells. J. Comp. Neurol. *242*:247–262.

Dacey, D.M. (1985b) Analysis of dendritic structure of cat retinal ganglion cells. Neurosci. Abstr. *11*:338.

Dacey, D.M. (1987) Identification of a dopamine-accumulating ganglion cell type in the cat's retina by *in vitro* fluorescence. Neurosci. Abstr. *13*:1057.

Dacey, D.M. (1988) Dopamine-accumulating neurons revealed by *in vitro* fluorescence display a unique morphology. Science *240*:1196–1198.

Dann, J.F., and E.H. Buhl (1987) Retinal ganglion cells projecting to the accessory optic system in the rat. J. Comp. Neurol. *262*:141–158.

De Lima, A.D., and W. Singer (1987) The serotoninergic fibers in the dorsal lateral geniculate nucleus of the cat: Distribution and synaptic connections demonstrated with immunocytochemistry. J. Comp. Neurol. *258*:339–351.

Enroth-Cugell, C., J.G. Robson, D.E. Schweitzer-Tong, and A.B. Watson (1983) Spatio-temporal interactions in cat retinal ganglion cells showing linear spatial summation. J. Physiol. (Lond.) *341*:279–307.

Famiglietti, E.V., Jr., and H. Kolb (1976) Structural basis for ON- and OFF-center responses of retinal ganglion cells. Science *194*:193–195.

Farmer, S.G., and R.W. Rodieck (1982) Ganglion cells of the cat accessory optic system: Morphology and retinal topography. J. Comp. Neurol. *205*:190–198.

Freed, M.A., and P. Sterling (1988) The ON-alpha ganglion cell of the cat retina and its presynaptic cell types. J. Neurosci. *8*:2303–2320.

Fukuda, Y., C.-F. Hsiao, M. Watanabe, and H. Ito (1984) Morphological correlates of physiologically identified Y-, X-, and W-cells in the cat retina. J. Neurophysiol. *52*:999–1013.

Fukuda, Y., and J. Stone (1974) Retinal distribution and central projections of Y-, X-, and W-cells of the cat's retina. J. Neurophysiol. *37*:749–772.

Illing, R.-B., and H. Wässle (1981) The retinal projection to the thalamus in the cat: A quantitative investigation and a comparison with the retinotectal pathway. J. Comp. Neurol. *202*:265–285.

Keyser, K., L.R.G. Britto, and H.J. Karten (1987) Catecholaminergic ganglion cells in the retina of the pigeon. Neurosci. Abstr. *13*:1058.

Kolb, H., R. Nelson, and A. Mariani (1981) Amacrine cells, bipolar cells and ganglion cells of the cat retina: A Golgi study. Vision Res. *21*:1081–1114.

Leventhal, A.G., J. Keens, and I. Törk (1980) The afferent ganglion cells and cortical projections of the retinal recipient zone (RRZ) of the cat's 'pulvinar complex'. J. Comp. Neurol. *194*:535–554.

McGuire, B.A., J.K. Stevens, and P. Sterling (1986) Microcircuitry of beta ganglion cells in cat retina. J. Neurosci. *6*:907–918.

Osborne, N.N., T. Nesselhut, D.A. Nicholas, S. Patel, and A.C. Cuello (1982) Serotonin containing neurons in vertebrate retina. Neurochem. Int. *3*:171–176.

Oyster, C.W., E.S. Takahashi, M. Cilluffo, and N. Brecha (1985) Morphology and distribution of tyrosine hydroxylase-like immunoreactive neurons in the cat retina. Proc. Natl. Acad. Sci. USA *82*:6335–6339.

Rodieck, R.W., and M. Watanabe (1986) Morphologic diversity in the ganglion cell projection to different zones within the cat lateral geniculate nucleus. Neurosci. Abstr. *12*:1038.

Saito, H.-A. (1983) Morphology of physiologically identified X-, Y-, and W-type retinal ganglion cells of the cat. J. Comp. Neurol. *221*:279–288.

Sandell, J.H., and R.H. Masland (1986) A system of indoleamine-accumulating neurons in the rabbit retina. J. Neurosci. *6*:3331–3347.

Stanford, L.R. (1986) W-cells in the cat retina: Correlated morphological and physiological evidence for two distinct classes. J. Neurophysiol. *57*:218–244.

Stone, J., and R. Clarke (1980) Correlation between soma size and dendritic morphology in cat retinal ganglion cells: Evidence of further variation in the gamma-cell class. J. Comp. Neurol. *192*:211–217.

Stone, J., and Y. Fukuda (1974) Properties of cat retinal ganglion cells: A comparison of W-cells with X- and Y-cells. J. Neurophysiol. *37*:722–748.

Sur, M., and M. Sherman (1982) Linear and non-linear W-cells in C-laminae of the cat's dorsal lateral geniculate nucleus. J. Neurophysiol. *47*:869–884.

Tauchi, M., and R.H. Masland (1984) The shape and arrangement of the cholinergic neurons in the rabbit retina. Proc. R. Soc. Lond. [Biol.] *223*:101–119.

Tauchi, M., and R.H. Masland (1985) Local order among the dendrites of an amacrine cell population. J. Neurosci. *5*:2494–2501.

Tauchi, M., and R.H. Masland (1986) Subpopulations of catecholaminergic neurons in the rabbit retina. Neurosci. Abstr. *12*:198.

Törk, I., and J. Stone (1979) Morphology of catecholamine-containing amacrine cells in the cat's retina, as seen in retinal wholemounts. Brain Res. *169*:261–273.

Tornqvist, K., C. Hansson, and B. Ehinger (1983) Immunohistochemical and quantitative analysis of 5-hydroxytryptamine in the retina of some vertebrates. Neurochemistry *5*:299–308.

Ueda, S., N. Ihara, and Y. Sano (1985) The organization of serotonin fibers in the mammalian superior colliculus: An immunohistochemical study. Anat. Embryol. (Berl.) *173*:13–21.

Ueda, S., and Y. Sano (1986) Distributional pattern of serotonin-immunoreactive nerve fibers in the lateral geniculate nucleus of the rat, cat and monkey (*Macaca fuscata*). Cell Tissue Res. *243*:249–253.

Vaney, D.I., S.P. Collin, and H.M. Young (1988) Dendritic relationships between cholinergic amacrine cells and direction-selective retinal ganglion cells. From NATO Advanced Research Workshop on "The Inner Retina." In press.

Vardi, N., P. Masarachia, and P. Sterling (1988) Association of alpha cell dendrites with cholinergic amacrine processes. Neurosci. Abstr. *14*:604.

Voigt, T., and H. Wässle (1987) Dopaminergic innervation of AII amacrine cells in mammalian retina. J. Neurosci. *12*:4115–4128.

Wässle, H., B.B. Boycott, and R.-B. Illing (1981a) Morphology and mosaic of on- and off-beta cells in the cat retina and some functional considerations. Proc. R. Soc. Lond. [Biol.] *212*:177–195.

Wässle, H., and R.-B. Illing (1980) The retinal projection to the superior colliculus in the cat: A quantitative study with HRP. J. Comp. Neurol. *190*:333–356.

Wässle, H., L. Peichl, and B.B. Boycott (1981b) Morphology and topography of on- and off-alpha cells in the cat retina. Proc. R. Soc. Lond. [Biol.] *212*:157–175.

Wässle, H., T. Voigt, and B. Patel (1987) Morphological and immunocytochemical identification of indoleamine-accumulating neurons in the cat retina. J. Neurosci. *7*:1574–1585.

Weiler, R., and J. Ammermüller (1986) Immunocytochemical localization of serotonin in intracellularly analyzed and dye-injected ganglion cells of the turtle retina. Neurosci. Lett. *72*:147–152.

Wilson, P.D., M.H. Rowe, and J. Stone (1976) Properties of relay cells in the cat's lateral geniculate nucleus: A comparison of W-cells with X- and Y-cells. J. Neurophysiol. *39*:1193–1209.